

Experimental Implementation of Lorentz Force Actuators for Hydrodynamic Drag Reduction

by

Corey Jaskolski

B.S. Physics and Mathematics
University of Wisconsin - Stevens Point, 2000

SUBMITTED TO THE DEPARTMENT OF ELECTRICAL ENGINEERING AND
COMPUTER SCIENCE IN PARTIAL FULFILLMENT OF THE REQUIREMENTS
FOR THE DEGREE OF

MASTERS OF SCIENCE IN ELECTRICAL ENGINEERING AND COMPUTER
SCIENCE
AT THE
MASSACHUSETTS INSTITUTE OF TECHNOLOGY

MAY 2002

(May 2002)

©2002 Massachusetts Institute of Technology. All rights reserved.

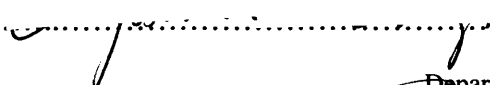
The author hereby grants to MIT permission to reproduce
and distribute publicly paper and electronic
copies of this thesis document in whole or in part.

Signature of Author:.....



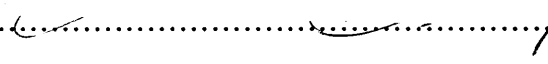
Department of Electrical Engineering and Computer Science
May 8, 2002

Certified by:.....



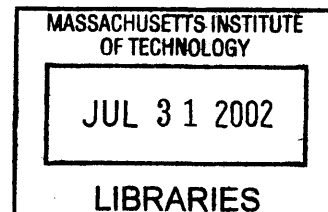
Chryssostomos Chryssostomidis
Department Head, Ocean Engineering Department
Thesis Supervisor

Accepted by:.....



Arthur C. Smith
Chairman, Department Committee for Graduate Students

ARCHIVES



Experimental Implementation of Lorentz Force Actuators for Hydrodynamic Drag Reduction

by

Corey Jaskolski

Submitted to the department of Electrical Engineering and Computer Science on May 8, 2002 in Partial Fulfillment of the Requirements for the Degree of Masters of Science in Electrical Engineering and Computer Science.

Much of the current research in turbulent drag reduction centers on controlling locally individual streamwise vortices. These techniques involve complex closed loop control systems that become difficult or impossible to implement in practice. Extensive numerical simulation has suggested that introducing streamwise vorticity in the form of a transverse unsteady excitation can reduce drag far more effectively than spanwise vorticity control and would only require simple open loop control making it far easier to implement.

In this work we implemented the above concept using Lorentz force actuators consisting of alternating pairs of electrodes and magnets. Specifically, we used a transverse oscillating square current waveform, and conducted experiments in a weakly conductive sodium nitrite solution. Detailed velocity profiles using laser Doppler velocimetry (LDV) were obtained in the 1 to 3 m/s range, and preliminary direct force measurements were made with piezoelectric force sensors.

The primary findings of this work are:

- Drag reduction of up to 37% was observed, in agreement with direct numerical simulations (DNS).
- Input power was observed to vary inversely with flow speed.
- Dependence of the effect on frequency was in agreement with DNS with the optimum period at about $T^+ = 100$.
- Change in drag was observed to be non-monotonic with respect to current as predicted by DNS.
- At higher speeds the amplitude range for which drag reduction occurred was observed to increase.
- Electrode thickness, which influences the Lorentz force penetration depth into the fluid, was shown to not be as critical as suggested by DNS.
- Conductive polymer coating of the electrodes was shown to dramatically reduce corrosion and electrolysis.

These results are the first experimental manifestation of large turbulent drag reduction using electro-magneto-hydro-dynamic (EMHD) excitation. In addition, this work was done at speeds several times faster than any other previous EMHD experiments. They point to net power savings at speeds above about 8 m/s and to robustness of this approach for real world applications.

Thesis Supervisor: Chryssostomos Chryssostomidis
Title: Department Head, Ocean Engineering Department

Acknowledgements

I would like to thank George Karniadakis, Chryssostomos Chryssostomidis, Richard Kimball, and Vasileios Symeonidis for helping me in the research and writing of this thesis. I would also like to thank my family and friends for their years of support and encouragement. In particular I can always count on Dawn and Roger Brodzeller, Jeremy Jaskolski, John and Adonna Jaskolski, and Chris Randlett.

The one person I could never have done this without is my fiancée, Ann Gajewski. I will be forever grateful for the days of patience and understanding that it must take to live with an MIT grad student. Ann, I hope I make you feel half as lucky to be with me as I do to be with you, because if I do... I've got you hooked for life!

Table of Contents

1. Introduction	8
1.1 Background	8
1.1.1 Drag Reduction	8
1.1.2 Numerical Simulations	8
1.2 Motivation	13
1.3 Thesis Objective	13
1.4 Guide to This Thesis	14
2. Phase 1 Experiment	15
2.1 Experiment overview	15
2.2 Electronic Equipment	16
2.2.1 Electrode Plate	16
2.2.2 Power Switching	17
2.2.3 Power Supply	18
2.3 Test Plate	19
2.3.1 Mechanical Design	19
2.3.2 Magnets	20
2.4 Laboratory Facilities	21
2.4.1 Water Tunnel	21
2.4.2 Laser Doppler Velocimetry	22
2.5 Experimental Challenges	23
2.5.1 Water Tunnel Corrosion	23
2.5.2 Electrolysis and Oxidation	24
2.6 Results	27
2.6.1 LDV Measurements	27
2.6.2 Implementation Issues	32
3. Phase 2 Experiment	35
3.1 Experiment Overview	35
3.2 Experiment Design	37
3.2.1 Electrical	37
3.2.2 Mechanical	39
3.2.3 Force Measurement	39
3.3 Results	45
3.3.1 LDV Measurements	45
3.3.2 Direct Force Measurements	51
4. Conclusions and Future Work	56
4.1 Conclusions	56
4.2 Contributions of This Work	56

4.3 Future Work	57
References	62
Appendix	63

List of Figures

Figure 1-1: Modeled magnetic field	9
Figure 1-2: Modeled electric field	10
Figure 1-3: Lorentz force	10
Figure 1-4: Drag reduction simulation	11
Figure 1-5: Simulated mean velocity profile	12
Figure 1-6: Simulated rms velocity profile	12
Figure 2-1: Experiment mounted in tunnel	20
Figure 2-2: Magnet pole orientation	21
Figure 2-3: Water tunnel diagram	22
Figure 2-4: NaNo ₃ conductivity plot	24
Figure 2-5: Electrolysis near electrode plate	25
Figure 2-6: Electrode corrosion	27
Figure 2-7: Typical full velocity profiles	28
Figure 2-8: Near wall velocity profiles	28
Figure 2-9: No power linear fit	29
Figure 2-10: Active electrode linear fit	30
Figure 2-11: Phase 1 results	31
Figure 2-12: Change in du/dy	32
Figure 2-13: Rms velocities	33
Figure 3-1: Force sensor	41
Figure 3-2: Force sensor calibration procedure	43
Figure 3-3: Force sensor calibration curve	44
Figure 3-4: Velocity sweep	45
Figure 3-5: 1.5 m/s amplitude sweep	46
Figure 3-6: 3.0 m/s amplitude sweep	47
Figure 3-7: Both $T^+=100$ amplitude sweeps	48
Figure 3-8: $T^+=135$ amplitude sweep	49
Figure 3-9: 1.5 m/s near wall velocity profile	50
Figure 3-10: 3.0 m/s near wall velocity profile	50

Figure 3-11: Force sensor output	52
Figure 3-12: Processed force sensor signal	53
Figure 3-13: Amplitude sweep with force sensors	54

1. Introduction

1.1 Background

1.1.1 Drag Reduction

Numerical simulations over the past 10 years as well as a significant body of experimental evidence have led to the concept that controlling locally individual streamwise vortices can reduce hydrodynamic drag on a body moving through the water [1,2,3,4,5]. Several strategies have been employed to realize this drag reduction. Many of these implementations have involved either riblets or complex closed loop control of the streamwise vortices. Unfortunately, there are significant problems with each of these techniques, which limit their practicality in implementation. The riblet technique, although fairly easy to implement since it is an open loop process, results in limited drag reduction (<10%) [2]. On the other hand, closed loop control methods become difficult or impossible in practice due to their inherent complexity.

A new technique for accomplishing drag reduction through the control of vortices has recently been modeled and numerically analyzed by mathematician, George Karniadakis of the Brown University Center for Fluid Mechanics. His technique involves the introduction of streamwise vorticity into the turbulent boundary layer using Lorentz forces generated by a series of electro-magnetic tiles [5]. Extensive numerical simulations have shown that a significant drag reduction can be realized using this technique [4,5]. Also, since this method will involve only open loop control, it will not suffer from the same implementation difficulties that make other vorticity control schemes impractical at high Reynolds numbers.

1.1.2 Numerical Simulations

The technique that we implemented was extensively modeled using direct numerical simulations done mainly by George Karniadakis's group at Brown University. Although cases involving spanwise sinusoidal traveling waves were the focus of many of these simulations, other models explored the use of other force functions [2,3]. In our case, we

implemented spanwise vorticity by using Lorentz forces that were produced by oscillatory square wave currents that propagated in the streamwise direction.

The technique used to produce the Lorentz forces in the numerical simulations was to place a large number of long thin electrodes with equal sized magnets between them at the interaction surface for a flow. The magnets are orientated so that one row has its north pole in the plane of the electrodes and the following row has its south pole in the plane of the electrodes. The electrodes are powered such that at a given time, one electrode is positive and the following is at a negative potential of the same magnitude as its positive neighbors. For the purposes of the direct numerical simulations, this pattern of +,N,-,S repeats itself infinitely along the direction of the flow. Modeling this steady state configuration gives a Lorentz force in the spanwise direction with a characteristic amplitude which depends both on the excitation potential and penetration depth which is determined by the size of the electrodes. [5]

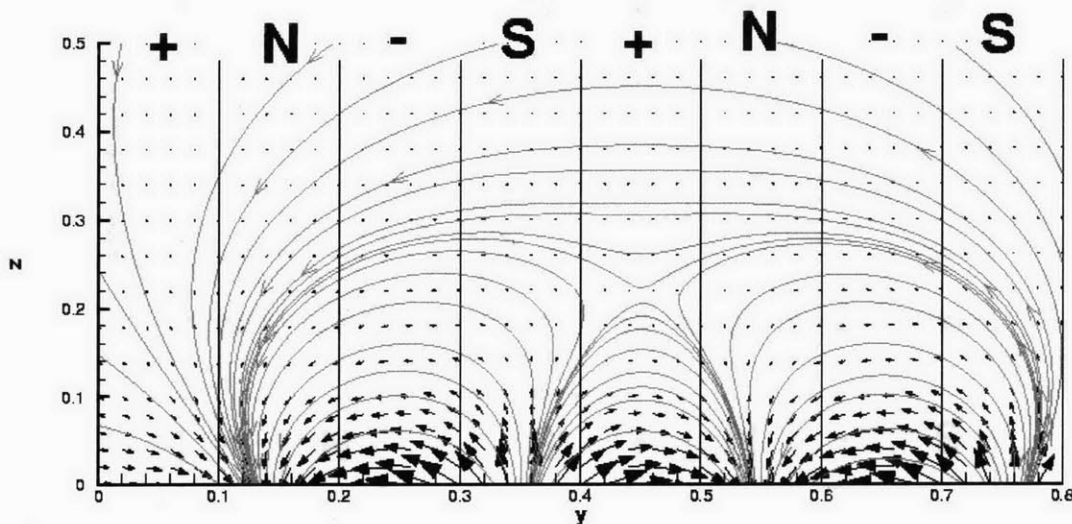


Figure 1-1: Modeled magnetic field. In our case both the electrodes and magnets were .125" wide. This slice in the plane of the electrode array is taken at a height equivalent to 0.1 the height of an electrode above the electrode plate.

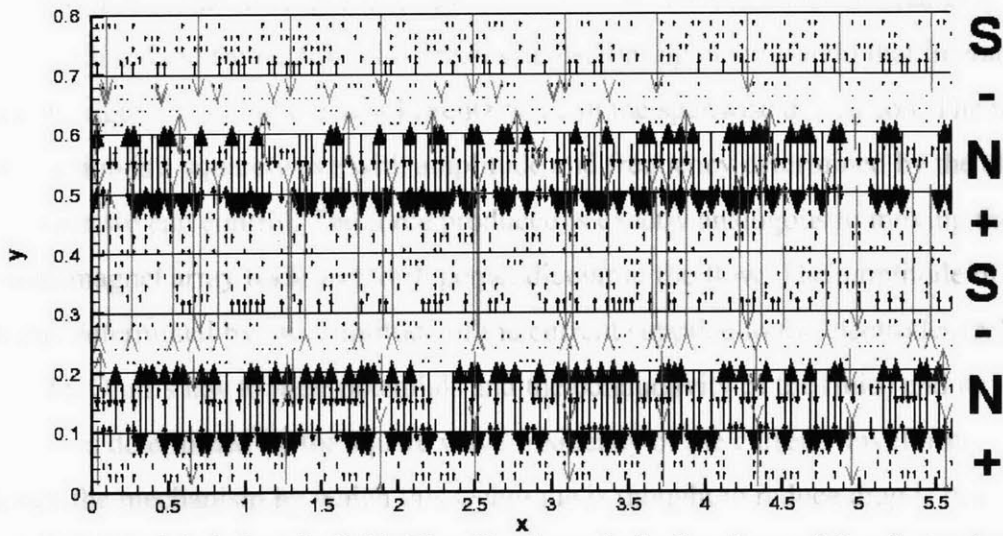


Figure 1-2: Modeled electric field. The slice is again in the plane of the electrodes at 0.1 electrode units above the plane.

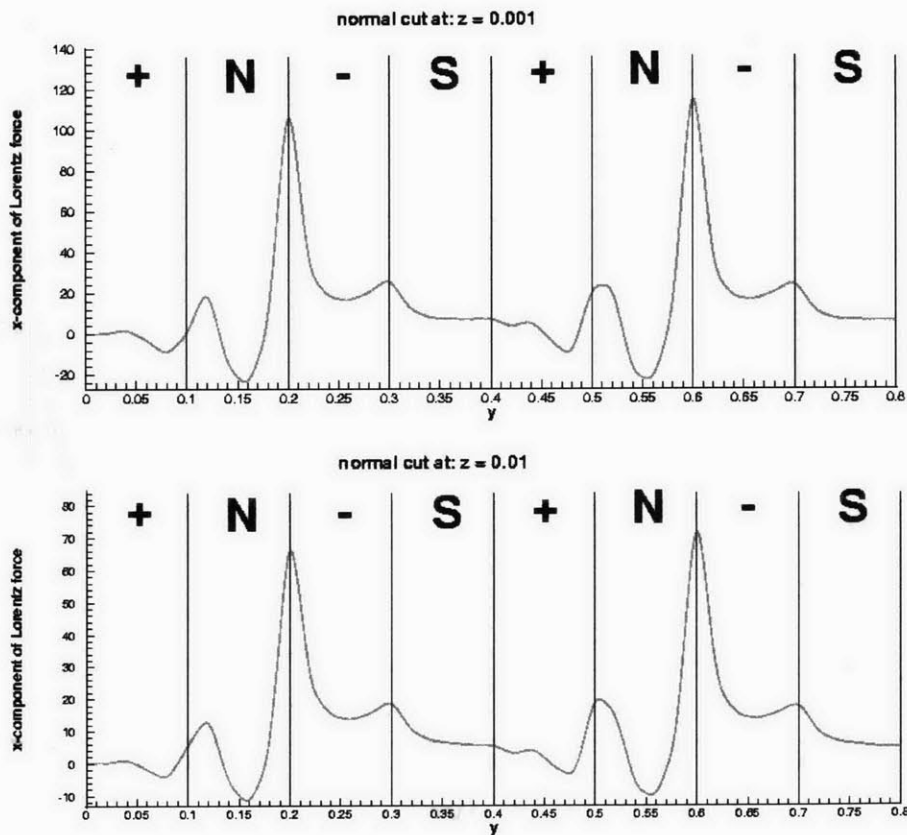


Figure 1-3: Modeled spanwise Lorentz forces. Note the falloff of the force the higher the slice is above the electrode plane; this is due to the penetration depth of the induced force.

From this basic configuration, the electrodes are then modeled as changing polarity with a fixed frequency. This creates an oscillating electric field that interacts with the fixed magnetic field to create a Lorentz force in the spanwise dimension. The induced force function is a square wave with amplitude and frequency determined by the electric field, which we can control. The force produced is exactly analogous to moving the electrode/magnet array back and forth perpendicular to the flow. The amplitude of this motion is determined by the amplitude of the current supplied to the electrodes (related linearly by Ohm's law to their potentials and the conductivity of the fluid) and its frequency is determined by the square wave frequency of the current waveform. Although the mechanism by which this technique is thought to reduce drag is not completely understood, its effect on the suppression of streaks have been extensively investigated in the numerical simulations [1,2,3,4].

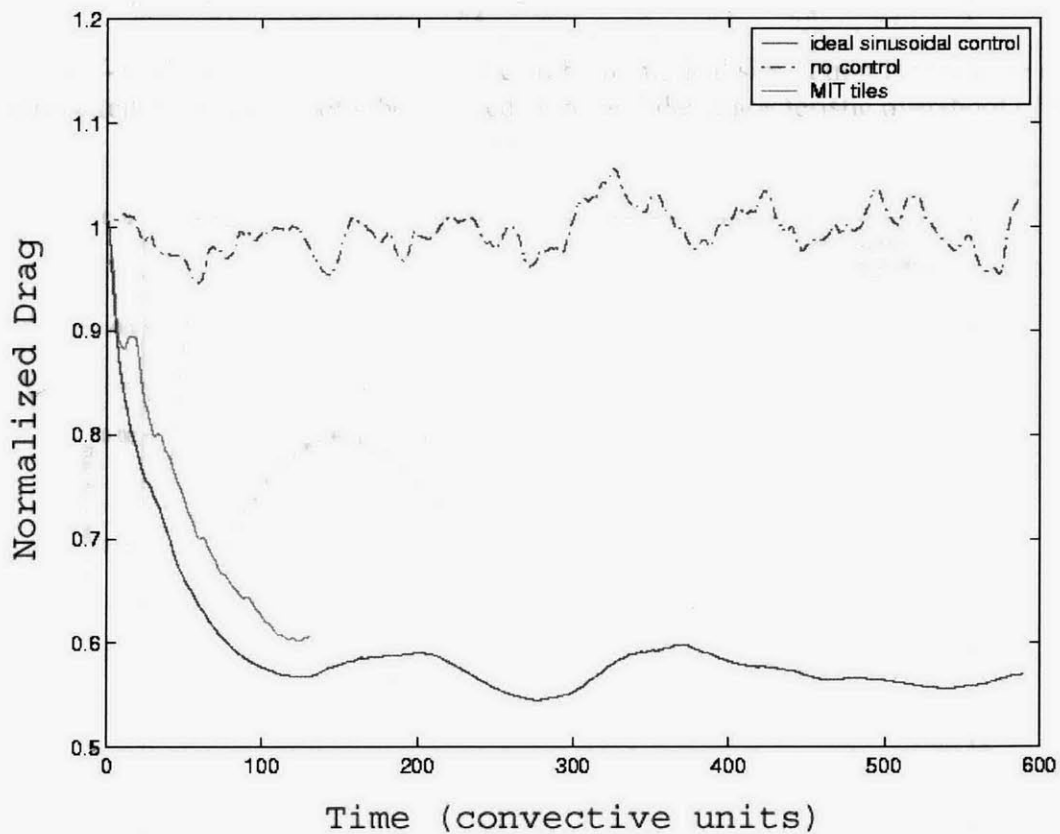


Figure 1-4: Effects of the spanwise Lorentz force oscillating as a stationary sine wave (MIT tiles) on our electrode plate as predicted by the direct numerical simulations in comparison to the effects on an idealized electrode plate. Although the square wave DNS is not yet complete, it is expected to be slightly more effective than the stationary sine wave excitation.

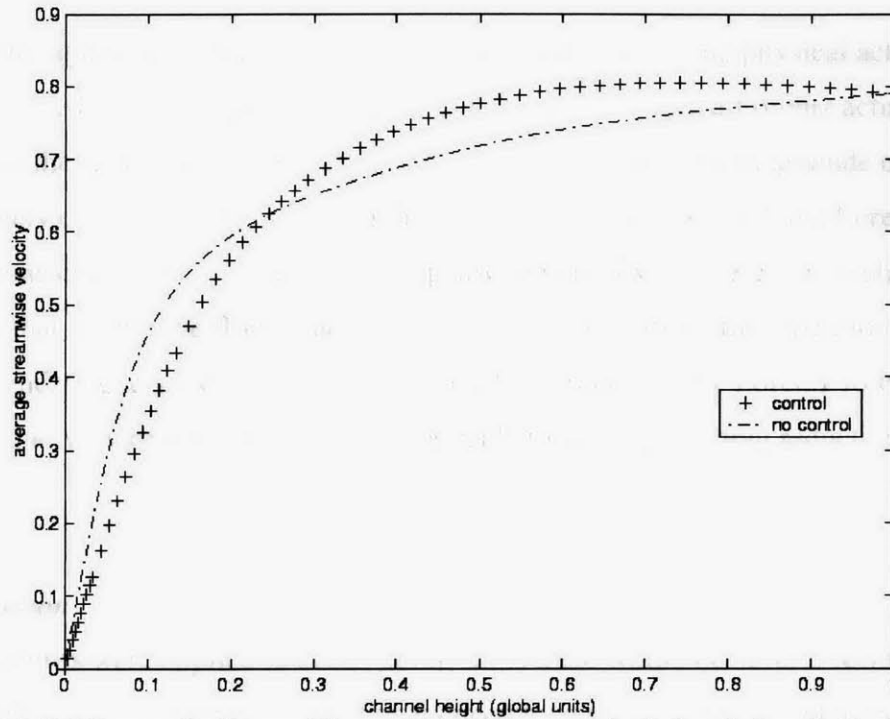


Figure 1-5: Mean velocity profile predicted by numerical simulation for both the no control and control cases. Note both the reduced slope and the characteristic overshoot of the control case.

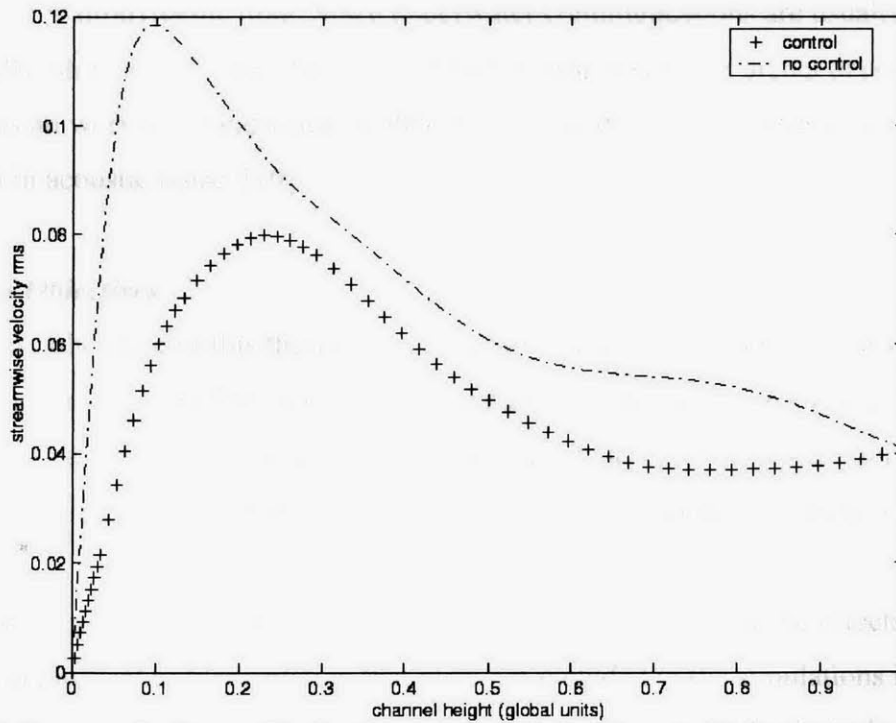


Figure 1-6: rms velocity profile for the uncontrolled and controlled case as predicted by DNS. The lower peak value and spreading of the profile in the control case is typical.

Although other groups have implemented techniques using physical actuators to manipulate the boundary layer in the spanwise dimension, using a Lorentz actuator to accomplish the spanwise forcing has several advantages. First, the magnitude of the force is completely controllable by adjusting the current amplitude. Second, the Lorentz force is a non-contact method of producing the spanwise vorticity, so there are no physical structures that disrupt the flow in any other direction. Because of the repetition of the electrode and magnets sections, the streamwise force produced by Lorentz force actuation cancels out to very nearly zero, which is desirable to accomplish drag reduction.

1.2 Motivation

If these benefits were applied to ocean going ships there would be several rewards. Most significantly, fuel consumption would be reduced by a factor proportional to the drag reduction. Not only does this reduce costs, but would also considerably reduce emission of pollutants. A more subtle benefit is the acoustic noise reduction that accompanies a reduction in hydrodynamic drag. Since underwater communications are usually done acoustically, ship noise is one of the largest factors responsible for signal degradation and limitations on workable bandwidth. A 30% decrease in drag corresponds to a 12dB reduction in acoustic noise. [10]

1.3 Thesis Objectives

The primary objective of this thesis is the experimental implementation of the drag reduction technique modeled by George Karniadakis' group at Brown University. Secondary goals include characterization of the Lorentz actuators, optimization of the effect (in terms of power expended), and the exploration of parameters used in the simulations.

The primary objective demands that we discover and account for the effects occurring in an actual physical implementation that were not included in the simulations in order to make the calculations tractable. Some of these considerations include electrolysis of the conductive solution, oxidation of the electrode plates, and interactions between

neighboring electrode-magnet pairs. There are several purposes for characterizing the Lorentz actuators beyond gauging the level of drag reduction observed. As the Lorentz actuators produce significant forces in a non-contact, non-intrusive manner, there are many conceivable applications for them. Some examples include micro water jets and manipulations of small-scale flow.

1.4 Guide to This Thesis

This thesis is arranged in four parts with an appendix. This section gives an introduction to the concepts and overview of the goals of this research. Also in this section is a summary of the numerical simulations that led to this work.

Section 2 details the design, implementation, and results of the first phase of this work. A detailed description of the apparatus used and constructed is included along with a brief overview of the water tunnel facilities and measurement equipment used. After discussing the results of this phase, Section 2 closes with consideration of the experimental issues that need to be resolved to increase the reliability and repeatability of this experiment.

Section 3 describes the second phase of this work. Here we discuss how we used the results and issues of phase 1 to design and construct a better experiment. This section describes the many changes and enhancements made to our original experiment. This section also contains our findings about control parameters versus efficiency as well as how the effect varies with the water velocity. Finally, the results of the experiment as well as the issues we had to contend with are considered.

The final section of this thesis examines the contribution that this work has made to the field. Thoughts on enhancing this experiment as well as ideas for future work are given. Appendix A contains the electrical schematics, printed circuit board layouts, and mechanical drawings for the apparatus designed for this experiment.

2. Phase 1 Experiment

2.1 Experiment Overview

In Phase 1 of this work we implemented the drag reduction technique suggested by the direct numerical simulations of George Karniadakis' group at Brown University. Their work indicated several variations of traveling and oscillatory waveforms that were shown to produce significant (up to about 35%) drag reduction through the direct numerical simulations [2,3]. For this phase we decided to use an oscillating square current waveform that reversed polarity every half cycle. This waveform produced a similar degree of drag reduction in the numerical simulations and was significantly easier than the traveling wave method to implement experimentally. This technique contrasts the other drag reduction through spanwise vorticity studies currently being done, which mostly focus on generating a traveling sinusoidal waveform in the spanwise dimension [3,4].

After deciding on the current waveform, we had several key experimental challenges that needed to be solved. Solving these implementation issues formed the vast majority of the work as we moved from numerical simulation to experimental verification. Among these issues were high current control and switching, electrode board design, electrode oxidation, water electrolysis, test facility corrosion, and drag measurement.

In order to handle the high currents needed to make this technique work, we chose to purchase a high current power supply and design an IGBT based h-bridge switcher to produce the negative half cycles of the current waveform. After dealing with the control and thermal issues, this solution worked quite well for producing clean square waves well past the frequencies which we were interested in. Although we only tested the square waveforms, modifications to our design would allow us to explore some of the other usable waveforms [6].

We designed a custom electrode board, which was realized as a printed circuit board. The plates used in this experiment consisted of twenty pairs of electrodes. Each electrode was 3.175mm wide by 304.8mm long. One ounce copper traces were used in order to allow us to pass high currents without damage to the electrodes. With a total electrode

area of 38.71 mm we could achieve current densities of 775 A/m² at 30A. We had significant problems with oxidation of the electrodes during the experiment, which limited repeatability in this first phase.

Another issue we faced was the potential corrosion of the MIT water tunnel that served as our test facility. This 6000-gallon water tunnel is constructed almost entirely of steel. Our initial proposal suggested mixing several hundred pounds of salt (NaCl) with the water to match the conductivity of seawater. The corrosive effects of this solution would have demanded that we quickly run our experiments in a 24-hour period and then purge and flush the tunnel to minimize the corrosion. Fortunately, we found an alternative to this destructive method by using sodium nitrite in place of the salt.

In order to match the experiment with the numerical simulations, we needed to run at fairly low speeds (about 1 m/s). The reason for this is that at higher speeds, direct numerical simulations become very difficult and computer intensive to perform. Because we were running at such a low velocity, 30% drag reduction would result in a net change in force of less than 0.1 Newtons. Measuring this small of a force with the technologies in place at the water tunnel test facility was not possible. To get around this limitation, we decided to use Laser Doppler Velocimetry (LDV) to measure the water velocity inside the boundary layer. By calculating the derivative of the velocity at the wall we could find the local shear stress at the measurement point from which we could infer the relative drag on our test plate without resorting to direct force measurements. This method, although widely used, gives us the relative change in shear force at the measurement point, which is not necessarily linearly related to the total drag on the plate. Because of this issue, the changes in drag reported should be viewed as an upper bounds and not the exact change in drag over the entire plate.

2.2 Electronic Equipment

2.2.1 Electrode Plate

The electrode plate was the key to the formation and control of the Lorentz force. Since the magnetic field polarity and strength was fixed by using permanent magnets, the electric field created between electrodes completely determined the character of the induced spanwise force. In our design, the electrodes would change in potential and

polarity over time when driven by the power control electronics. In order to perform these functions, the electrode plate needed to have several specific characteristics that made it unlikely that we would find a commercially available product. Because of this, we designed the electrode plates at MIT.

Construction of the electrode plate was accomplished by the fabrication of a printed circuit board with unmasked copper tracks serving as the electrodes. The board consisted of 40 electrodes on the top surface and 2 power buses on the bottom surface. One-ounce copper was used in order to allow the electrodes to handle the sustained high currents that would be present during testing. The board we designed is 279.4mm x 330.2mm including the mounting perimeter around the electrode section. Of that area, 254mm x 304.8mm is the active electrode surface and space for the magnets while the edges are used for mounting to the test plate described in section 2.3. The total amount of copper electrode area was 38.71 mm². The printed circuit board design is reproduced in the appendix at a 1:2 reduction. The electrode plates used in this phase were printed and etched by Advanced Circuits.

2.2.2 Power Supply

To produce the electrical fields needed for this experiment in the highly conductive sodium nitrite solution, we required high current but relatively low voltage. There are several commercially available supplies that perform well in this range. We chose the Hewlett Packard HP-6671A (all of the HP test and measurement equipment is now sold and supported by Agilent). This supply has a voltage range of 0-8V and can source currents of up to 220A. It has a built-in GPIB interface so it may be controlled remotely via a GPIB enabled computer. Originally it was hoped that we could create low (<5Hz) frequency waveforms of nearly arbitrary shape by sending frequent voltage update commands to the supply. Although there was some success with this idea, further calculations showed we might need frequencies of square or sine waves of up to about 50Hz for our electrode dimensions and resulting force penetration depth at 1 m/s water velocity. At these higher frequencies, updating the power supply's setting to match the desired function does not work due to limitations on the ability of the output to track the commanded function because of the supply's capacitance.

2.2.3 Power Switching

Because changing the power supply output remotely cannot produce waveforms of greater than a few Hertz, we needed to implement a switching technique to create the waveforms of interest. Although the ability to create arbitrary waveforms would have been optimal, we settled for square waves to reduce the cost and complexity of the setup. Section 4.3 on future work suggests how one could implement other waveforms of interest. Methods for generating pulse width modulated and pulse train waveforms would build upon the IGBT switcher we have already completed and would allow us to generate a much broader set of waveforms.

In general, high current power supplies have a fixed polarity. For us this means that we could generate a square wave that goes from 0 to +V volts (0V to 8V with the HP-6671A). Numerical simulations have shown that this waveform will not create the desired effect, but a square wave that swings from negative to positive (-8V to 8V for example) has been shown in simulations to cause drag reduction at appropriate frequencies and amplitudes. To allow for the negative part of the square wave we needed to construct an h-bridge switch.

Like the electrode board, many requirements on the power switching subsystem made it unlikely that we would find a commercial solution at a reasonable cost. For this reason we built an insulated gate bipolar transistor (IGBT) based h-bridge switch. The IGBT we used was the CM100BU-12H model from Powerex. These modules contain 4 IGBT switches already configured in the h-bridge topology. Although the CM100BU-12H modules are rated at 100A, at the low voltages we are using the safe operating area extends to 200A if proper cooling allowances are made to keep the junction temperature below 150 degrees Centigrade [7]. To keep the module as cool as possible, it was attached to an extruded fin heat sink equipped with a high airflow volume cooling fan. Further cooling through the use of a liquid cooled heat sink plate is possible to further extend the safe operating area of this device if it were to prove necessary.

Gate drive circuitry for the module consists of four sets of DC-DC converters and gate drive modules as well as some logic and power circuitry. The DC-DC converters are used to change the bus voltage (12V nominal) to +15 and -8V supplies. For any type of

transistor, the conductivity of the collector-emitter path depends (to some extent) on the gate potential. The +15 and -8 supplies provide gate potentials high enough above the threshold switching potentials of the IGBTs to ensure that they switch on and off hard [7]. The DC-DC converters used in this design are the M57145L-01 converters manufactured by Powerex for use in IGBT gate driver circuits. The schematics for this gate drive are given in the appendix.

To control the IGBT gate, we used four M57962L gate driver modules (again manufactured by Powerex) which provide both a TTL to gate drive potential level shift as well as several protective features. The TTL interface allows us to use 0-5V signals to control each individual IGBT. In this application a function generator is used to provide TTL square waves of adjustable frequency. This signal is also inverted using a Schmidt trigger hex inverter. The non-inverted signal is used to switch one half of the h-bridge (2 IGBTs) while the inverted signal controls the other half. This scheme insures that power always flows through the load (the water in our case). We recognize the possibility that this technique could cause a brief short in the IGBT module for the duration of the turn-off or turn-on time (whichever is greater) for the IGBTs. However, given the brevity of these times (nanoseconds), the module's short circuit handling capabilities, the current limiting of the power supply, the low operating frequency (5-100Hz), and the time delay imposed by the logic inverter gates, this effect has not posed a problem for us [7].

2.3 Test Plate

2.3.1 Mechanical Design

The test plate is the fixture installed in the water tunnel test section to hold the magnets and electrode plate. The test plate consists of a rounded leading edge followed by 27 inches (0.69m) of flat plate before the electrode plate. The purpose of this inactive flat section is to establish a fully developed turbulent boundary layer before the active region.

There were several key issues to consider when designing the plate. Since the numerical simulations all assumed a well behaved, well defined magnetic field we needed to avoid using metals because of their magnetic field altering effects. Another consideration was that we needed support ridges built into the recessed magnet holding area to keep the .4 Tesla magnets from reorientating one another. These ridges greatly

increased the complexity of the machining work that was needed to complete this part. Because of its neutral magnetic properties as well as its ease of machining we chose to use Delrin for the plate. A steel back plate was added to the bottom of the test plate in order to provide a closed path for the magnetic fields to eliminate interference with the structured fields near the electrode board. The bolts used to retain the electrode board and steel back plane are plastic while the bolts used to mount the plate to the tunnel test section are made from threaded fiberglass rod with plastic nuts.

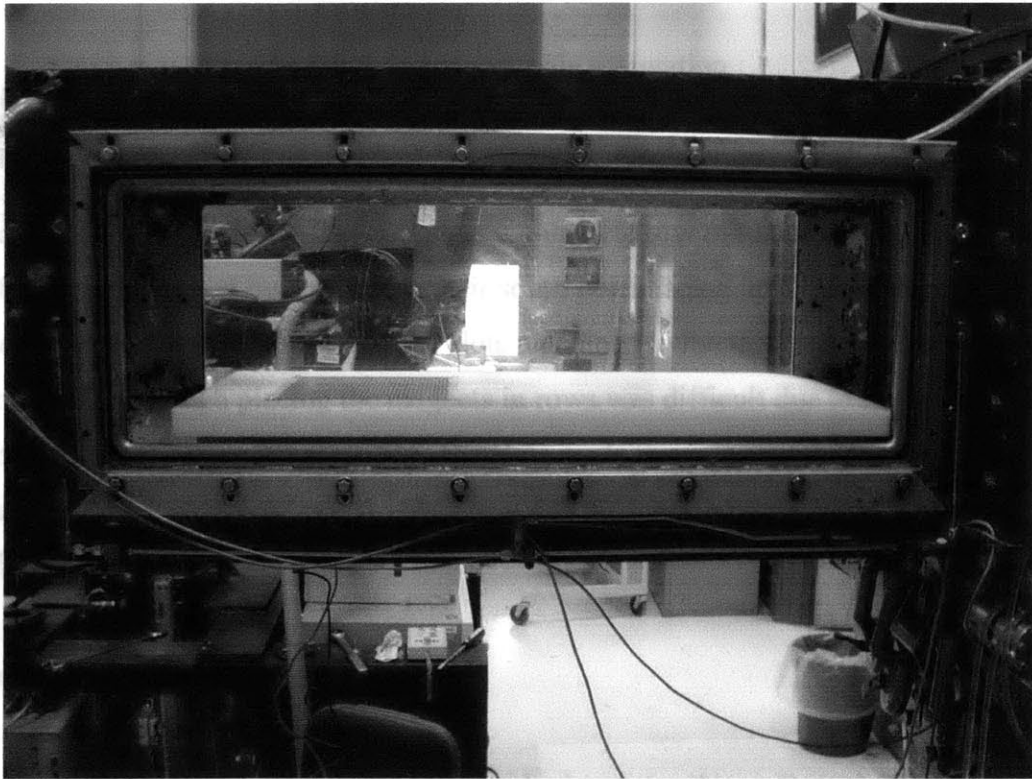


Figure 2-1: Assembled board in water tunnel test section. The electrode plate is visible mounted on the test plate.

2.3.2 Magnets

The magnets which were used to populate the test plate were Neodymium Iron Boron rare earth magnets from Indigo Instruments. These magnets were coated with a Nickel plating to prevent corrosion due to moisture, a real problem with rare earth magnets. They have a magnetic field of about .4 Tesla on their surface and are 2 inches long by 1 inch deep by .125 inches wide. The poles axis is such that the north pole is on the top half (nearest the electrode plate) of the 1 inch depth and the south is on the bottom.

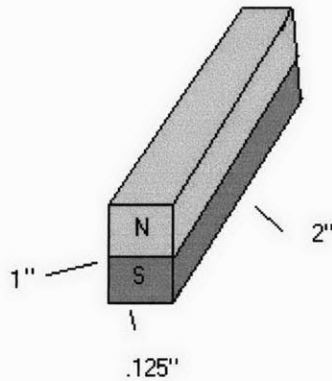


Figure 2-2: Magnet pole orientation

To get the 12" span of magnets we needed to insert 6 of them end to end into the test plate. This was done such that there was a complete row of magnets with their north poles facing up followed by a row with their south poles facing up. This basic unit was repeated until the 39 rows formed by the slots machined in the test plate were populated with magnets. Although placing the magnets in rows was difficult due to the repulsive force between magnets in the same row, the slots made this considerably easier. The combination of the retaining grooves and the steel back plate ensured that the magnets were firmly held in place.

2.4 Laboratory Facilities

2.4.1 Water Tunnel

The facility used for our tests was the MIT Hydrodynamics Water Tunnel. This tunnel was built in 1938 primarily for the purpose of testing ship propellers. It holds 6000 gallons of water and spans two stories in MIT building 3. The test section in which experiments are run is about 1.2m by .5m and is accessed by four removable windows, which allow for mounting of experiments in any orientation. Drag and flow data can be taken with the lab's direct force sensors, Laser Doppler Velocimeter (LDV), or Particle Image Velocimetry system (PIV). Driven by a large impeller, water can be pushed through this test section at velocities up to 10 m/s. One drawback of using this test facility is its fairly high freestream turbulence, which varies between 5% and 3%

depending on the running velocity. Improvements to the tunnel are ongoing which should reduce the freestream velocity below the 1% mark through the addition of turbulence suppressing mesh.

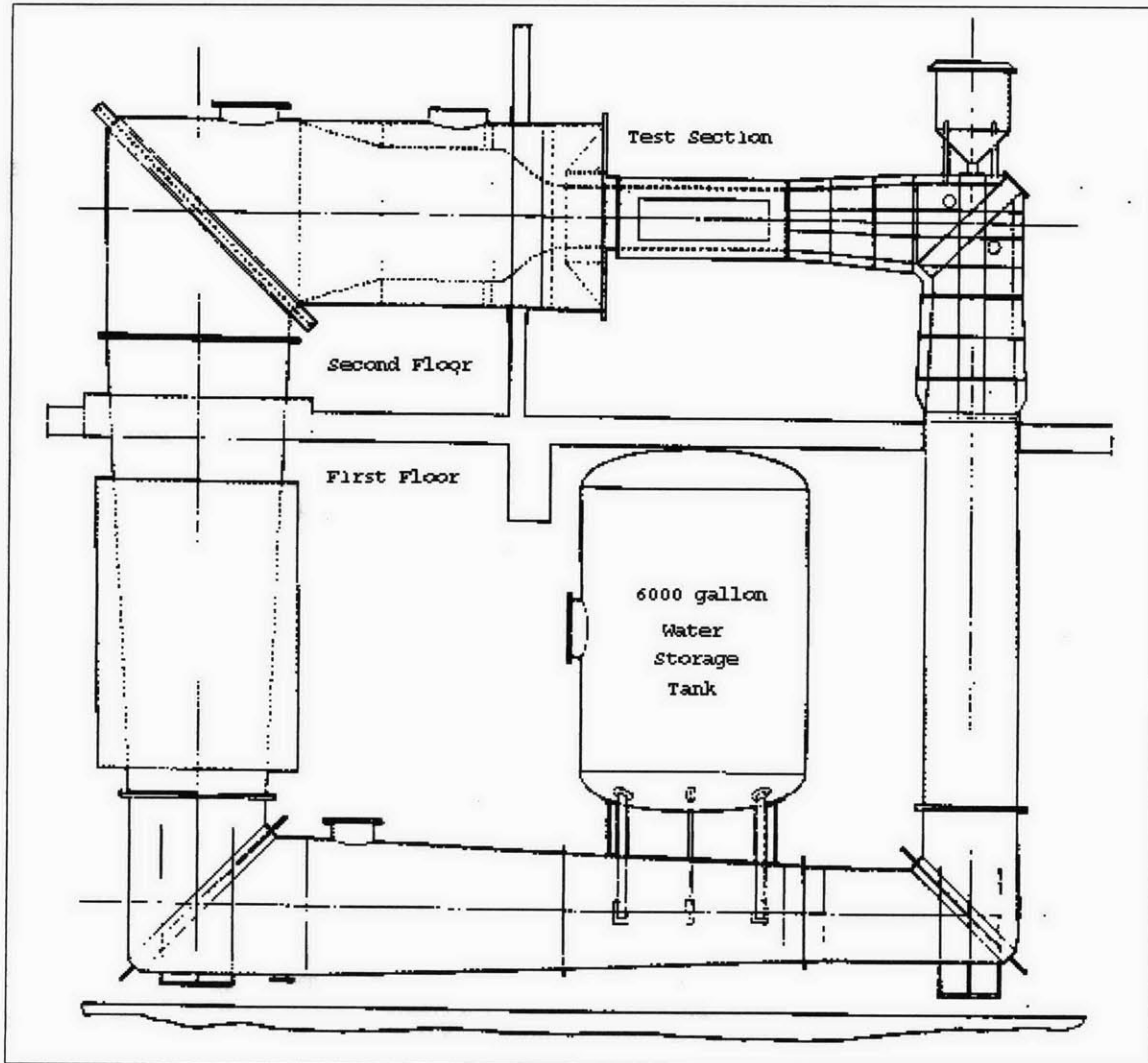


Figure 2-3: The MIT Marine Hydrodynamics Water Tunnel test facility.

2.4.2 Laser Doppler Velocimetry

Laser Doppler Velocimetry is a non-contact optical technique used to make very precise measurements of flow velocities. The basics of its operation involve focusing bisecting laser beams on the point of interest in the flow field and then collecting the reflected light. Due to the Doppler Effect, changes in the wavelength of the reflected radiation give the velocities of particles passing through the beams. The system in use at the MIT Marine Hydrodynamics Lab is composed of an Argon-Ion laser operated at 1.5W, photon

collection and amplification equipment, and data collection and processing through a Dantec FVA enhanced 58N40 LDV controller.

2.5 Experimental Challenges

2.5.1 Water Tunnel Corrosion

A major concern of the water tunnel research staff involved the necessity of a conductive fluid for the Lorentz force generation and the fact that the MIT Marine Hydrodynamics Laboratory Water Tunnel is made primarily of steel. Simply filling the tunnel with saltwater of the same salinity as seawater would have caused heavy corrosion of the tunnel over time. This problem is intensified because we would like the highest salinity possible as the greater the fluid's conductivity, the greater the achievable Lorentz force. To solve this problem, Richard Kimball, the MIT Ocean Engineering researcher that operates the Marine Hydrodynamics Laboratory, suggested that we consider adding sodium nitrite to the 6000 gallons of water in the tunnel rather than standard table salt (sodium chloride). We believed that this would not damage the tunnel as sodium nitrite was already being used in small quantities in the tunnel because of its corrosion inhibiting properties. After testing the effects of prolonged sodium nitrite exposure on the nickel coated magnets and steel samples, we found there to be no corrosion with sodium nitrate in comparison with the near total corrosion of similar items exposed to saltwater for the same duration.

To use sodium nitrite instead of seawater, we needed to find the concentration of sodium nitrite necessary to provide roughly the same salinity as seawater. The data shown below was gathered by dissolving sodium nitrite in tap water. Two electrodes were connected to a power supply set to 2V. By measuring the current as a function of the concentration of the sodium nitrite added to tap water we were able to compare the conductivity of the solution to our reference seawater sample. Roughly 1350 pounds of sodium nitrite mixed with the 6000 gallons of water in the tunnel would give us conductivity equivalent to that of seawater (corresponding to 27mA at 2V for the configuration we used). The experiment also showed that there are no problems with saturation of the sodium nitrite at this concentration.

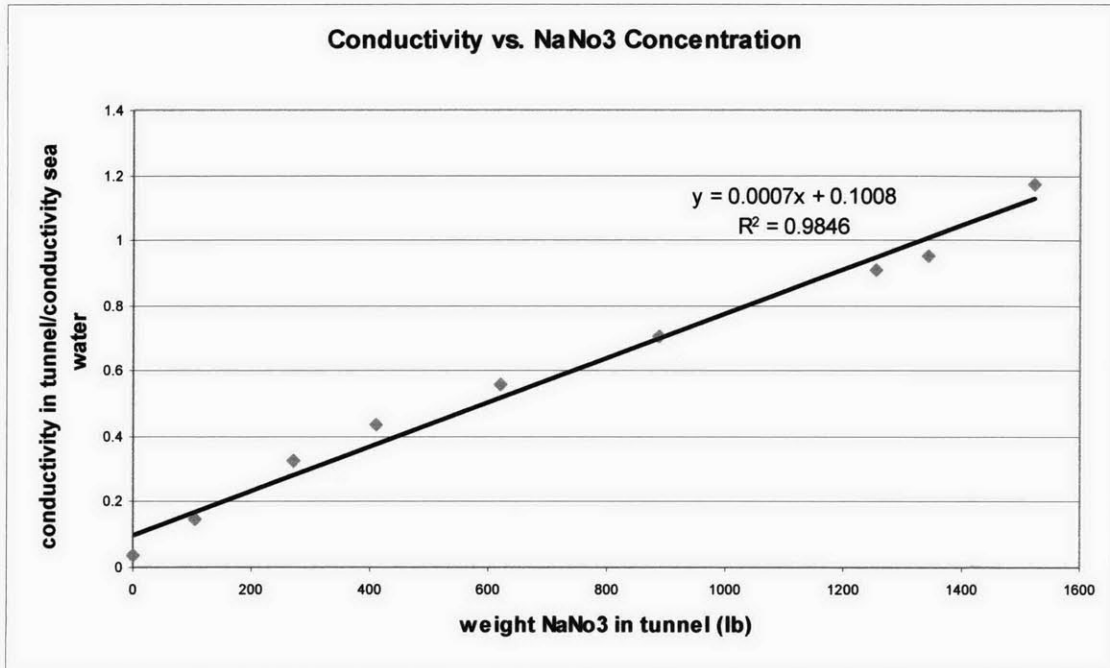


Figure 2-4: Conductivity of the solution in the water tunnel calculated for various amounts of sodium nitrite added to the tap water used to fill the tunnel.

2.5.2 Electrolysis and Oxidation

The biggest problem we faced in the implementation of this experiment was the electrolysis of water when potentials greater than the 1.23V threshold were applied across the rows of electrodes on the electrode plate. It became immediately apparent that at higher voltages (6V measured across the electrodes, corresponding to about 100A distributed over all the electrode pairs) the effects of electrolysis and oxidation of the electrodes would severely limit the feasibility of this experiment.

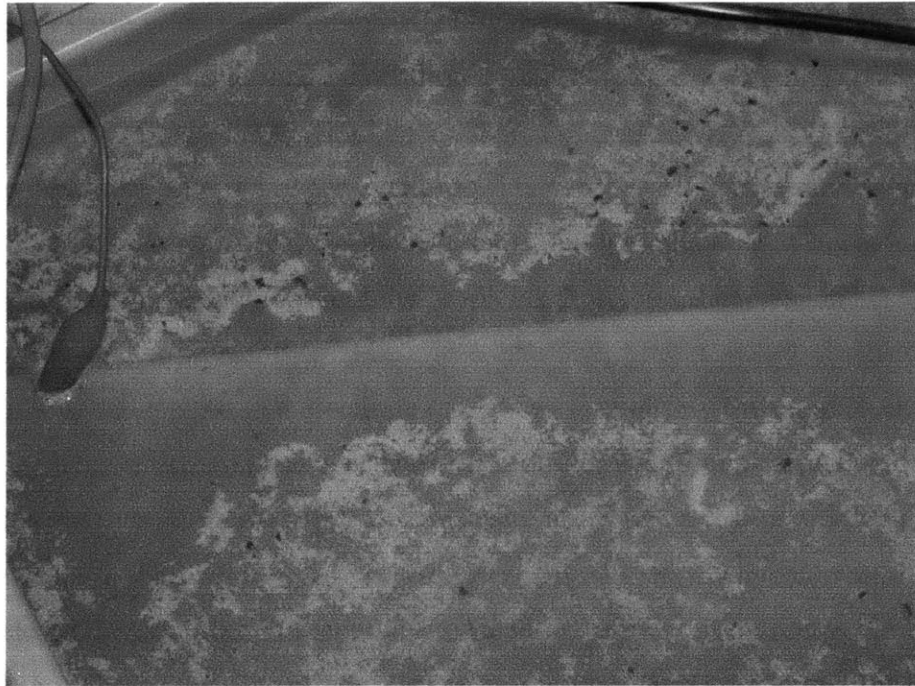


Figure 2-5: Heavy gas evolution near submerged electrode board due to electrolysis of water at voltages over 1.23V

Aside from the obvious issue of the electrodes oxidizing themselves completely away thus ending the experiment, the gaseous hydrogen and oxygen bubbles formed during electrolysis create several problems. The first of these is the potential accumulation of a large amount of hydrogen and oxygen gas somewhere in the water tunnel during extended run times. Fortunately, the tunnel is open to air in several places, providing a venting point for any gases.

The second, somewhat subtler problem, involves the measurement inaccuracies caused by the bubbles in the water stream since we are using Laser Doppler Velocimetry (LDV) to measure the mean flow velocity. LDV works by detecting light reflected off of nominally neutrally buoyant particles moving with the water stream. If the particles (bubbles in this case) are not neutrally buoyant, a z-component of velocity will be measured as the bubbles' buoyancy causes them to rise as they moves through the stream. Although this would probably be a fairly minor effect in the best case, at high voltages such a large number of bubbles are produced that taking useful LDV measurements would be virtually impossible.

All of these effects were observed while testing the power supply and circuitry in a steady state (no switching) mode. Fortuitously, as soon as the switching was enabled and the frequency above about .5Hz, bubble formation was significantly reduced. At 2Hz and above there was little if any gas evolution. There appears to be a time dependence in the electrolysis of salt water that was not expected, but will allow us to run at high (>1.23V) electrode potentials without the problems described above as long as we operate at frequencies greater than 2Hz.

Although it appears that electrode oxidation is intimately linked to electrolysis and that a reduction in the loss of electrode material follows from a corresponding reduction in gas evolution, we still had significant electrode corrosion problems. After even 30 minutes of activation we would experience moderately heavy corrosion to the exposed electrodes resulting in a small decrease in the amount of current achievable for a given voltage. These corrosive effects became more pronounced the longer the boards were powered.

Techniques for reducing oxidation of the electrodes include: coating them with a more resilient metal such as gold plating during the printed circuit board manufacturing process, coating with a conductive polymeric paint, or post manufacture treatment with conductive epoxy. We have attempted the conductive epoxy coating but had very limited success due to the difficulty of applying the silver laced epoxy. Its clay-like consistency made it nearly impossible to limit its application to the electrodes. Other groups working on EMHD experiments have told us that, in their experience, gold plating provides little if any additional protection for the electrodes. As a final option, the electrode boards used in phase 2 had a conductive polymeric paint masked to the copper electrodes during manufacture. In this phase we identified a local printed circuit board production house with these capabilities to use for the next segment of this work.

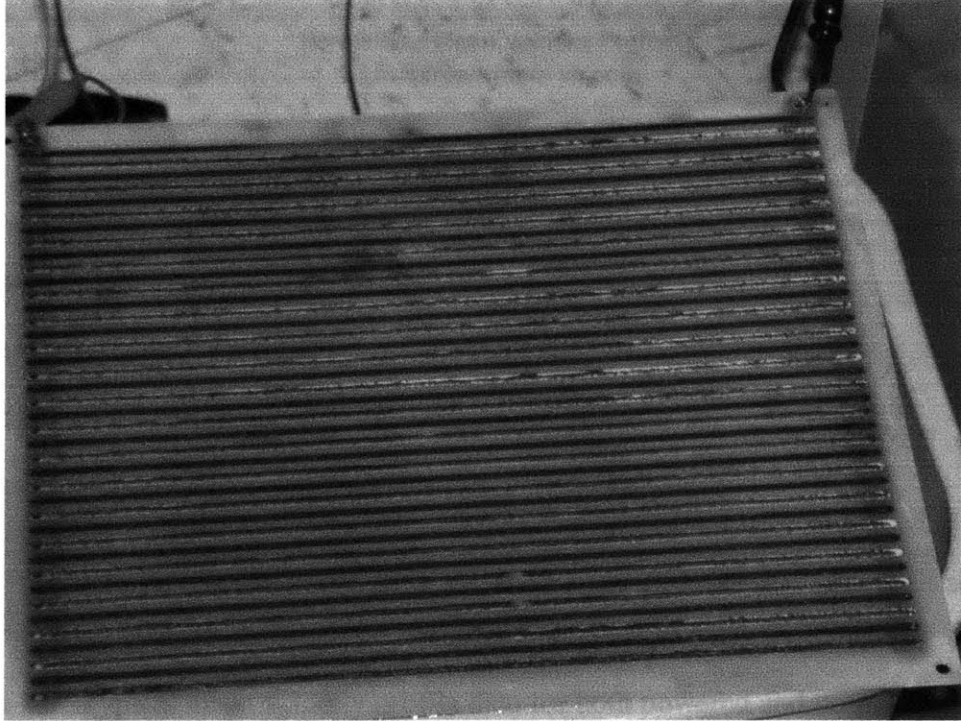


Figure 2-6: Effects of electrode plate oxidation.

2.6 Results

2.6.1 LDV Measurements

In total we performed 21 LDV measurements of the boundary layer velocity profile. Each measurement was taken at the downstream end on the electrode plate near its center. Of these runs, 6 were baseline cases without electrode activation and 15 were powered test runs. Each test series consisted of an un-powered run followed by between one and four powered runs at various frequencies. We preceded each set of powered runs with a new un-powered run to reduce the effects of day to day variations in the baseline velocity profile caused by factors such as electrode board oxidation and water tunnel velocity drift. The current amplitude used for each of the powered runs was between 20 and 30 amps. This was the maximum current we could draw from our 8V power supply given the water conductivity and the higher than expected losses in the switching electronics and wires. Each LDV run took between approximately 30 and 50 minutes as we were running at low speeds and did not “seed” the water tunnel with glass beads or any other substance.

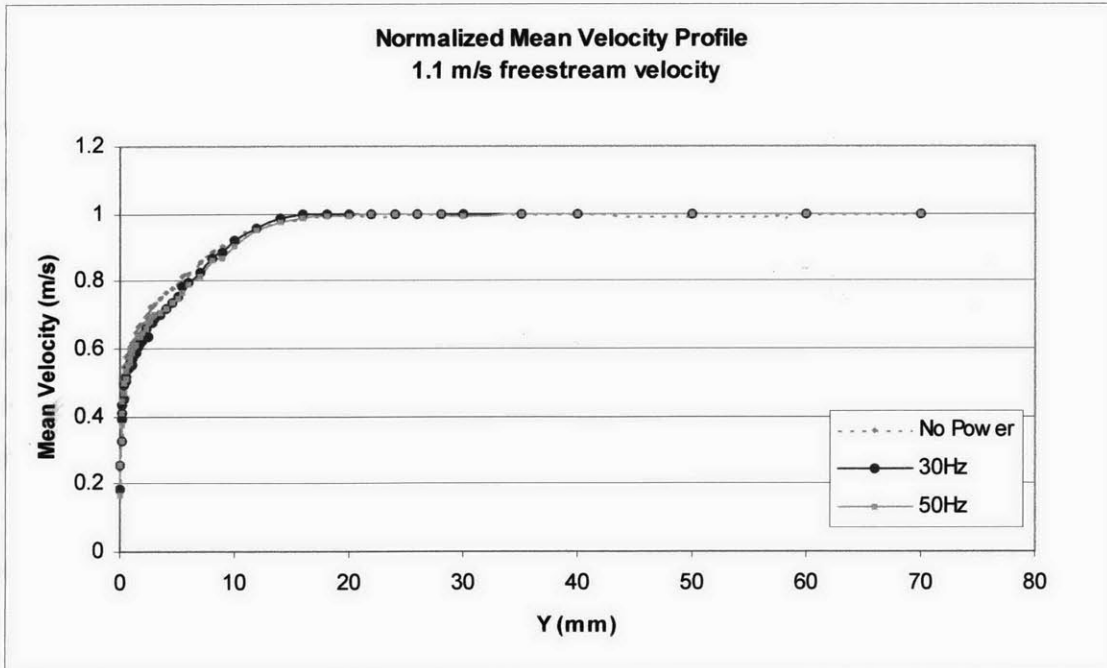


Figure 2-7: Typical mean velocity profile data for both powered and un-powered cases gathered using LDV.

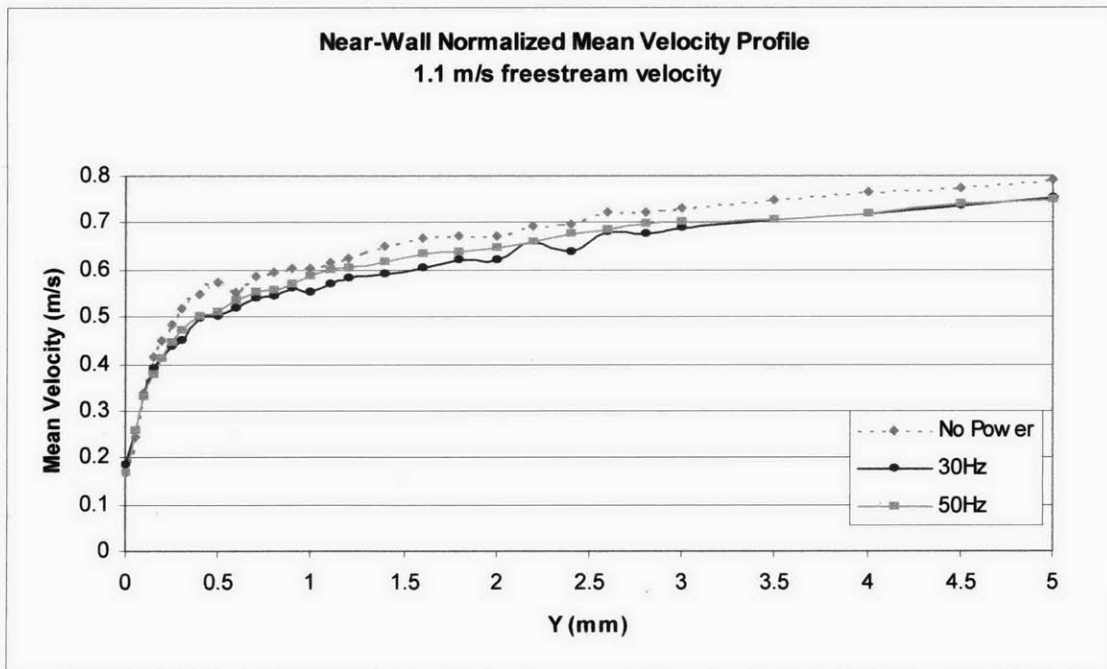


Figure 2-8: Detail of the near wall mean velocity profile as measured by LDV.

In order to calculate the relative drag on the electrode plate, we found the best linear fit to the first five near wall data points. The linear regressions were done using the

trend line feature in Microsoft Excel. Before doing this we removed the points closest to the wall that were clearly erroneous. This outlier removal is justified because to first order, the water velocity at the wall is zero (this is the no slipping assumption) [8]. For example, it was a common occurrence that the first point in a velocity profile would show an amplitude of greater than freestream velocity or even a negative velocity. The usual cause of these outliers is allowing at least one of the bisecting laser beams used in the LDV measurements to come partially in contact with the surface of interest. The measurement then interprets the interaction with the surface as moving particles, thereby giving erroneous data.

In each of the linear regressions, it could be suggested that using a mean velocity of zero at $z=0$ would have given an additional data point with a high degree of certainty. If so, using this point would give us a linear fit that more closely modeled the actual velocity profile at the wall. The reason we did not utilize this technique is that it is difficult to tell exactly where $z=0$ is with enough certainty to have allowed us to claim that the addition of the point (0,0) would increase the validity of our linear model near the wall.

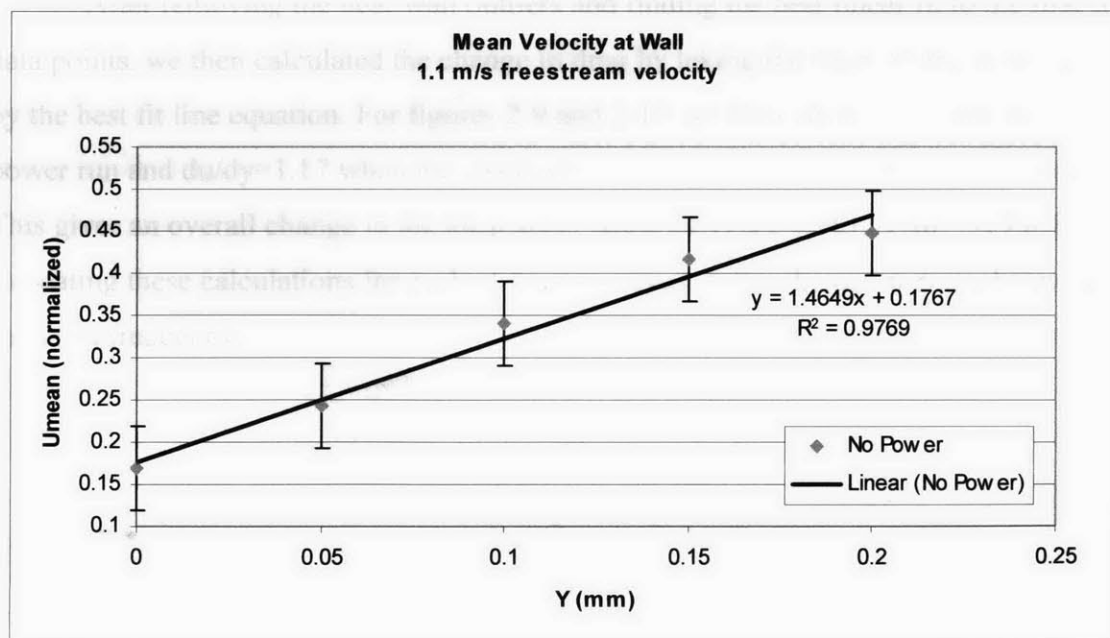


Figure 2-9: Linear fit of the first five data points for the no power run of figures 2-7 and 2-8. We get du/dy from the slope given in the linear equation for the trend line. The 5% error bars indicate the estimated uncertainty due to freestream turbulence and other factors.

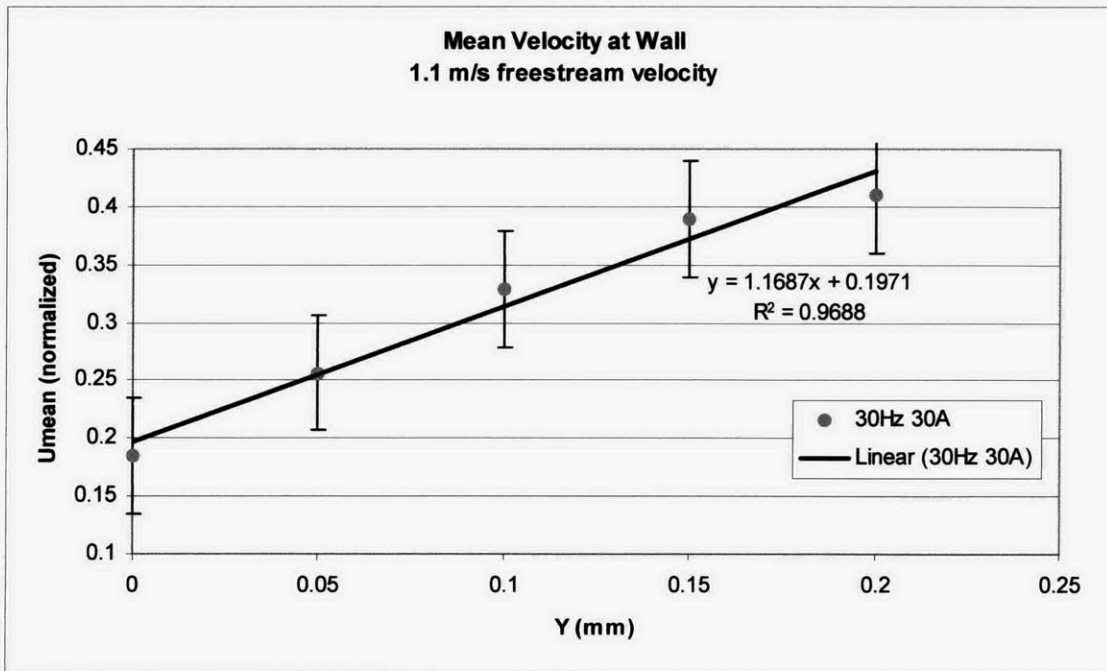


Figure 2-10: Best fit line to the first five points of the 30Hz data from figures 2-7 and 2-8.

After removing the near wall outliers and finding the best linear fit to the first five data points, we then calculated the change in drag by taking the ratios of the slopes given by the best fit line equation. For figures 2-9 and 2-10, we have $du/dy=1.46$ for the no power run and $du/dy=1.17$ when the electrode board is activated at 30Hz and 30 Amps. This gives an overall change in the local shear stress of $(1.17-1.46) / 1.46 = -19.8\%$. Repeating these calculations for each of the runs gives us the change in drag observed at each test frequency.

	Frequency (Hz)						
	5	10	15	20	30	50	100
Run 1	-22.1%	-9.2%	-17.4%	-27.9%	-20.2%	-27.7%	-23.4%
Run 2		-30.6%			-22.6%	-17.4%	
Run 3		-1.2%			-19.8%	+0.86%	
Average	-22.1%	-13.7%	-17.4%	-27.9%	-20.9%	-14.7%	-23.4%

Figure 2-11: Change in du/dy at various frequencies. All runs at 1.1 m/s freestream velocity and 25-30A total current depending on electrode board oxidation.

The results of the powered test runs that are summarized in figure 2-11 suggest several key points. The first is that we are indeed getting a significant amount of drag reduction. Over the 14 runs for which the electrodes were active, 13 show drag reduction to a level higher than the variability introduced by the tunnel turbulence (~5% turbulence). Although there are several incredulous data points such as 30.6% decrease in du/dy at 10 Hz and the 0.86% increase for the third trial at 50 Hz, it seems likely that we are seeing overall drag reduction in the general case.

The second point is that there are clearly other factors beyond the 5% tunnel turbulence causing variability, some of which include the electrode board oxidation, less than perfect fitting of the near wall velocity profile, and variations in the tunnel speed over the course of a set of runs. It is difficult to accurately gauge the errors introduced by these factors, but it is evident that considerably more runs along with finding and reducing these sources of variability will be needed to gain certainty in the observed values. Since we had done multiple runs at several of the frequencies, we can consider these values with more confidence.

The 10, 30, and 50 Hz frequencies were tested three times each at 1.1 m/s. In the 30Hz tests, the variation was extremely small, while the 10Hz and 50Hz runs show considerable variance mostly due to the single outlier in each set. Standard deviations are 15.2, 1.5, and 14.5 respectively.

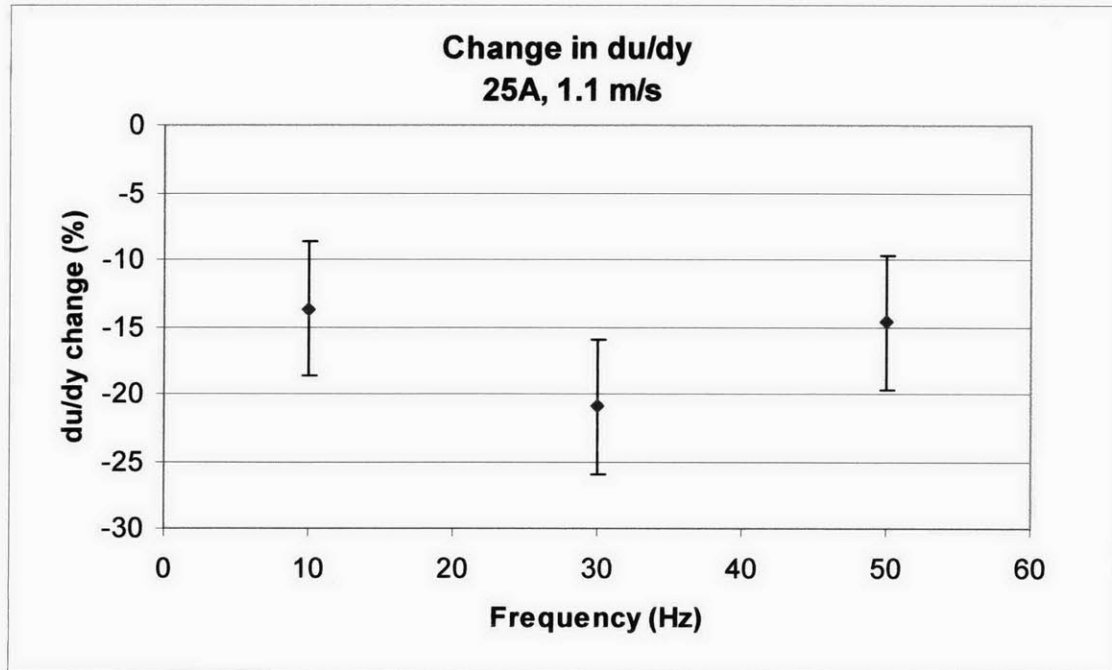


Figure 2-12: Change in local shear stress for each frequency run that was repeated three times. The 5% error bars indicate uncertainty due to tunnel turbulence.

2.6.2 Implementation Issues

As mentioned in the preceding sections, there were several major issues with implementation and testing. Those that affected the quality of the data and repeatability included: electrode board corrosion, high water tunnel turbulence, and water velocity drift. Other issues that limited some aspects of the study were mainly due to the maximum voltage attainable by our power supply being insufficient to provide over 30A with a fresh electrode board.

Water tunnel turbulence was as high as 5% of the free stream velocity when the tunnel was run at 1 m/s. This high level of turbulence both increased the variability in the observed velocity profiles and obscured important characteristics of the rms velocity profiles that would have helped us to ensure that we were actually seeing drag reduction. We had expected to see both a reduction in the peak amplitude of the rms velocity as well as a spreading out of the profile with the peak value moving further away from the wall in the case of drag reduction. This additional indicator of drag reduction is especially important to us since it would allow us to recognize data points that are contradictory or artifacts of the calculation procedure such as the -30.6% change in the local shear stress observed for the 10Hz case may be. Most of the published experiments that claim drag

reduction were done in facilities with a freestream turbulence of at or below 1% of the free stream velocity.

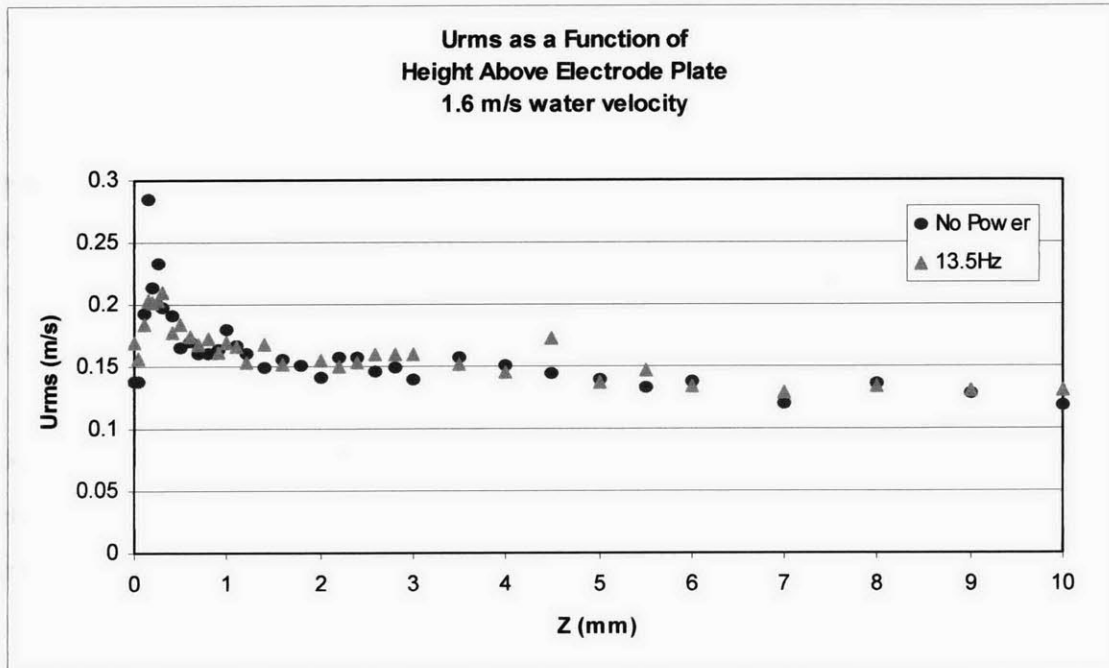


Figure 2-13: Near wall rms velocity data. The variability due to tunnel turbulence has obscured the shape of the curve at regions of interest. The change in du/dy at for the powered part of this run was -16.3%

Electrode board corrosion also greatly reduced the repeatability of this phase of the experiment. The corrosion of the board would typically increase the resistance of the electrodes by a factor of two to three after a few hours of running with the board activated. This effect reduced the amount of current we could pass between electrodes. Since this oxidation happened so quickly, not only did this reduce the board current between one run and the next, but in some cases also caused a significant reduction in current over the course of a single run since a typical LDV data session lasted as long as 45 minutes.

To attempt to reduce the effects of electrode board corrosion as much as possible, we cleaned the electrodes between each run with a wire brush. After vigorous cleaning we found that we could again get the electrode resistivity close to the original value for a new board. Unfortunately, the cleaning technique abraded the electrode surfaces and these flaws considerably increased the rate of electrode oxidation during following runs.

Another factor that considerably detracted from the repeatability of the experiment and the accuracy of the data was the drift in water tunnel velocity that would occur over the course of several hours. Since some of the LDV runs were quite long, this led to the freestream velocity changing by a small amount between runs. Although the change was fairly small (on the order of .05m/s), the effect on the slope of the velocity profile at the wall was larger since the drag increases as the cube of velocity. Each data set was normalized with respect to itself to preserve the qualitative shape of the profile and thus du/dy at the wall from which we inferred relative drag. In addition, the freestream velocity was measured and readjusted if it had drifted during a run.

The final implementation issue was that the HP6671A power supply that was used could not output a high enough voltage to explore some of the current regimes we were interested in. This oversight occurred because the losses in the switching circuitry and wiring were slightly higher than expected. This limitation kept us from adjusting for rising electrode board resistivity by simply stepping up the voltage to the electrode plate when we noticed a decrease in the current draw. Another drawback of the voltage limit was that we could not accurately measure the current with a shunt because we could not spare the voltage that needed to be dropped across the shunt to make this measurement.

3. Phase 2 Experiment

3.1 Experiment Overview

The second phase was designed to account for many of the shortcomings and issues discovered in the phase 1 work as well as to build on the concepts discovered during the first phase. Many changes and additions were made to increase the repeatability of the experiments and reliability of the measurements.

As noted previously, the issue that created the most trouble in the first phase was the oxidation of the electrode boards. This oxidation led to higher electrode resistance which in turn led to lower current densities from run to run. This undesirable variability in the current density greatly reduced the repeatability of the experiment. Although the level of the reduction in du/dy varied depending on the state of the electrode board, each time we saw results the direction was the same and indicated drag reduction as measured by the change in the derivative of the velocity at the wall. This observation made us feel that by solving the oxidation issue we would likely get drag reduction with every run for the proper combination of current and frequency. To inhibit the oxidation issues in this phase (as well as bubble formation) we coated the electrode boards with a conductive polymer during manufacturing.

Another area of enhancement involved acquiring a power supply with higher voltage output. Our original supply was limited to about 8 Volts. After accounting for electrical losses in the switching circuitry and wiring this left us with a maximum of 30A for a fresh electrode board in the sodium nitrite solution. Our newest power supply from Power Ten is capable of providing 40 Volts at 166 Amperes. This increase in power output allowed us to explore higher power regimes as well gave us more latitude by allowing us the option of increasing the voltage to account for oxidation effects if they were not completely prevented by the polymer coating. No changes to the switching electronics were needed to allow for higher voltages, as the IGBT module was capable of handling voltages of up to 600V.

To build on the experimental work and results of phase 1, we also designed a new electrode board with only half of the electrode thickness. This new board could be mounted on the original magnet array and would allow us to investigate the dependence

on the force penetration depth, which is linearly related to the electrode width for simple configurations and ideal fields. Direct numerical simulations indicated optimal results for electrode width of 10 to 20 wall units. Our electrodes were considerably larger than this as 20 wall units is only about .4mm at 1 m/s for our configuration and we could not find off-the-shelf rare earth magnets of this dimension. We had hoped that the smaller electrodes on the new board would increase the effect even though the magnets were still of the same size. Unfortunately, time constraints kept us from testing the new electrode board during this research.

The majority of the work in preparing for phase 2 was the designing, manufacturing, and assembling of a modified test plate instrumented with piezoelectric force sensors. This configuration was chosen to allow us to directly measure the drag force on the test plate in real time. Although the forces which we were attempting to measure were very close to the limits of the force sensors we used, this line of work was pursued to allow us to explore the effects of changing parameters on the amount of drag reduction observed with only seconds of measurement instead of the 45 minutes needed for LDV measurements in some instances. There were substantial challenges to implementing the direct force measurement system including mounting, transducer waterproofing, signal processing, and calibration.

After completing the changes to the experimental setup and instrumentation, we ran several different experiments. First, we attempted to reproduce the general results from phase 1 with better repeatability. Second, we attempted to explore both the current and frequency parameter spaces using the real-time feedback from the direct force measurement transducers. Finally, we focused on LDV measurement sweeps of the amplitude space at different water velocities while holding the frequency constant such that $T^+=100$ which gives the optimal frequency according to the direct numerical simulations. This last experiment was designed to help us understand how the optimal amplitude varies with water velocity, which is the key to calculating the velocity break-even point. Application of this technique at velocities faster than the break-even point would result in a net energy savings as the power supplied to the electrode array would be less than the power saved by the induced drag reduction.

3.2 Experiment Design

3.2.1 Electrical

Before solving any of the other implementation issues that we encountered in the phase 1 work, we first needed to greatly increase the repeatability of the experiment. The greatest source of this problem was the electrode board corrosion as previously mentioned. Kenny Breuer's group from Brown University had reported a significant decrease in both oxidation as well as bubble formation by coating the active regions of their boards, which they used for spanwise traveling wave excitement in channel flows, with a conductive polymer. The polymer used was PCR40384 from Metech, a specialty chemical manufacturer. This material contains palladium, which causes its price to fluctuate greatly with the market price of this element. The most common application of this material is its use as the resistive substrate in the construction of potentiometers. However, for thin coatings the resistivity was comparable to that of bare copper traces in our application.

The Metech material is typically applied in a screen-printing process similar to solder masking during printed circuit board manufacture. For this printing, we used a local board house, Multilab, with the capabilities and expertise to apply this coating to selected areas of the board. Other changes were made to the original electrode boards to further inhibit their corrosion. First, the bus tracks on the back of the boards were coated with non-conductive solder mask. Second, the vias that connected the individual electrodes to the power tracks were filled with the same mask material. This change was made to prevent oxidation of the copper coating inside the through-hole vias that would eventually lead to complete electrical disconnection of the affected electrode. A final alteration, at the suggestion of the Multilab engineers, was to layer the non-conductive mask material .005" onto the electrodes from all directions. This gave the polymer coating a better surface to adhere to, thus reducing the possibility of oxidation along the edges of the coated electrodes.

After the new electrode boards were manufactured and coated, we tested them to compare the corrosion and bubble formation against these effects on the uncoated boards. This test was done mixing a saltwater solution of 20g/liter as was done for the testing of the uncoated boards. A board identical to the original electrode plates except for the

coating and masking changes was placed in the solution and run at 30A for 1 hour. Upon inspection of the tested plate, we found that there was almost no evidence of corrosion to the electrodes in comparison to the extremely heavy corrosion seen on the uncoated boards tested under the same conditions. Also, during the trial the amount of bubble formation seemed to be significantly reduced for the coated electrodes.

The final change that we made to the electrical equipment was to replace the HP6671A power supply with a model from Power Ten that had a higher voltage output. The Power Ten 40V166A power supply was able to source 166A at 40V. By increasing our maximum voltage by a factor of five, we reaped several benefits. The most significant benefit was the ability to explore higher current regimes during testing. At 40V we would be able to easily provide the full 166A given the conductivity of the sodium nitrite solution we used in phase 1. However, when preparing for phase 2, a modest leak developed in the water tunnel filter pump. This pump was responsible for removing rust and flakes that would develop over several days of running the tunnel. Because it was deemed unusable at the rate it was leaking, we feared that after two to three days of running, the water might become rusty enough to preclude taking LDV measurements as the laser would not be able to penetrate the water to the desired measurement location. Because of this, we planned to completely drain and refill the 6000 gallon tunnel every few days, thereby losing the salts. To mitigate the cost of this procedure, we only added 800lb of sodium nitrite to the tunnel. This gave us a solution in the tunnel with roughly 60% that of seawater. Even after halving the solution conductivity, we were able to provide about 110A for maximum power supply voltage. Operating at 110A, our original electrode plate would have a current density of 2840A/m^2 while the newest board design would have a current density of 5680A/m^2 as the electrodes were one half the width.

Another benefit of using the higher voltage supply was that we were able to insert a current shunt between the supply and electrode boards in order to accurately measure current instead of solely relying on the power supply display. The shunt also allowed us to observe the current waveform, which enabled us to monitor the electrode board performance as well as verify that the current waveform closely matched the input voltage waveform. Several effects such as inductance of the wiring and capacitance of the

printed circuit board that forms the electrode plate contributed to the current waveform not matching the signal from the function generator exactly.

A final benefit of the higher voltage range was that we would now be able to account for falling conductivity if the boards still oxidized to some degree. Fortunately, the polymer coating solved this problem so well that we did not need to explore this alternate solution with the coated boards. In fact, after 10 days of testing, the electrode board conductivity did not change by a perceptible amount.

3.2.2 Mechanical

There were several mechanical modifications to the Delrin test plate in order to accommodate the mounting of the force sensors as well as to accommodate the possibility of direct characterization of the Lorentz actuators. For the force sensors to measure the total drag on the electrode plate, we needed to make certain that the force sensors were the only mechanical parts making any contact with the electrode plate. To accomplish this we had the electrode and magnet mounting section cut out with a precision water jet by Central Machining. This left us with a cassette comprised of the electrode board, magnets and mounting ridges, and the steel plate below the magnets. The Delrin test plate now had a hole in the downstream end with a few thousandth of an inch clearance when the electrode cassette was reinserted. To the bottom of the Delrin plate, we attached a 16" square steel plate that had four holes threaded for M12 bolts. Four piezoelectric force sensors (described below) were placed between the electrode cassette and the 16" steel plate. Four M12 bolts were used to fasten everything together. We added adjusting screws to the bottom of the test plate in order to raise or lower different corners of the electrode cassette to ensure that it was flush with the test plate so as not to disrupt the water flow. The power wires were passed through holes in the bottom of the test plate to the electrode cassette and coiled in a manner that reduced their absorption of forces in the streamwise direction.

3.2.3 Force Measurement

Since the slope of the velocity profile near the wall (du/dy) is actually a measurement of the local shear, it may not be a good indicator of overall drag on the plate [8]. One

potential solution to this problem would be to take many velocity profiles along the streamwise direction of the board and then integrate du/dy found in the viscous sublayer across the entire dimension. Unfortunately, given the time it takes to perform a single LDV measurement, this is not an easy solution to implement. To attempt to get around this problem and still get a single value for the total drag, direct force measurements are needed.

The direct measurement of hydrodynamic forces at relatively low speeds is not yet a well solved problem. Many different implementations have been attempted by different researchers. Some of the more common schemes involve the use of strain gauges, pendulums with optical angular displacement measurements, and accelerometers. The main complications that these techniques meet with include crosstalk between dimensions, waterproofing issues, and difficulty resolving small forces. In order to attempt a slightly different solution as well as a desire for readily available off-the-shelf components, we decided on piezoelectric force gauges.

The force gauges we used were 9146A SlimLine charge mode shear force sensors from Kistler Instruments. These transducers measure force by the accumulation of charge on two quartz elements. This charge is then converted to a measurable voltage by a charge amplifier, in this case the 5010B1 dual-mode adjustable gain charge amplifier from Kistler. In our configuration, we needed four sensors (one at each corner of the electrode cassette). To measure the sum of the forces in an easy manner, each sensor was connected to a 4-way summing box provided by Kistler. The output of the summing box was a single charge signal that was in turn passed to the charge amplifier.

Mounting the force sensors to the electrode cassettes was accomplished by passing an M12 hex head bolt through a countersunk hole in the cassette, through the center of the force sensor (which resembled a $\frac{1}{4}$ " thick washer), into threaded holes in the lower steel mounting plate that attached to the large Delrin test plate. Because the shear forces are transmitted to the sensors by means of friction, a modest amount of torque was applied to the bolts. Because of the small forces we were interested in measuring, we did not need to tighten the bolts to the standard pre-loading torque of 70 Newton-Meters. In fact, we found that sensor sensitivity and drift suffered as we tightened the bolts, so we only applied enough torque to secure the electrode cassette to the test plate.

The biggest consideration in mounting the sensors was that they were not rated as waterproof and we intended on submerging them in the sodium nitrite solution that fills the water tunnel test section. Representatives at Kistler told us that although they are only classified as “splash-proof”, we might not have much of a problem in submerging them a few feet underwater with even minimal waterproofing efforts. In an attempt to waterproof the sensor packages, we coated the entire sensor face as well as signal cable entry point with silicone sealant. This solution would not have been an option if we were concerned with measuring large forces, as the silicone coating would definitely interfere with the frictional transmission of large forces to the sensor.

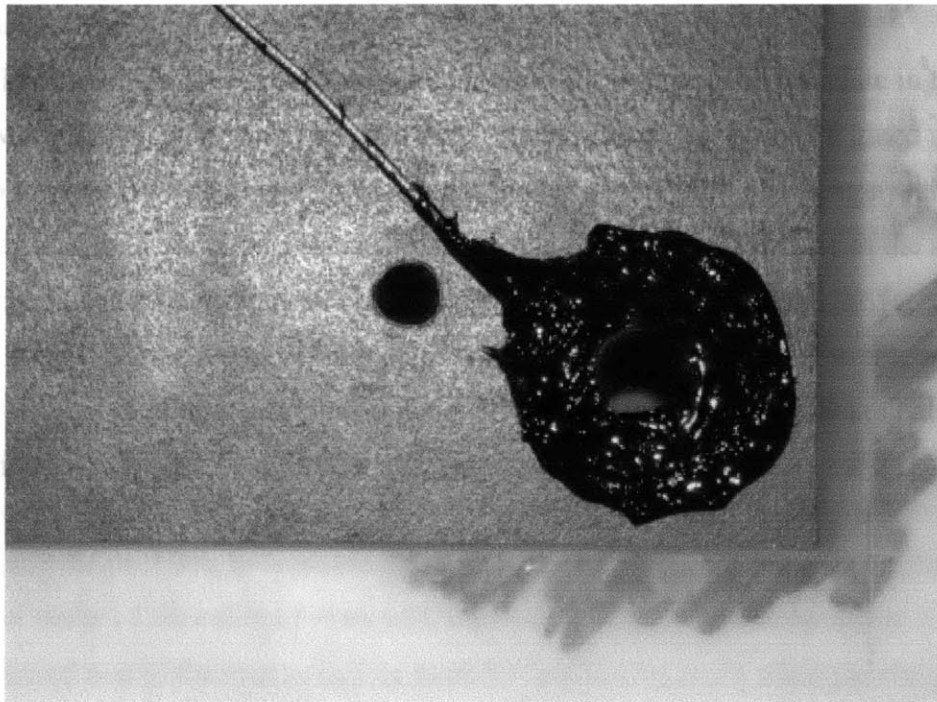


Figure 3-1: Force sensor in recess into which the electrode cassette fits. In actuality, the sensor is rotated so the shear force axis is parallel to the signal cable.

After the sensors were mounted into the test plate, we proceeded to calibrate them. Initial efforts immediately confirmed that although we could resolve as little as 30 grams quite easily, we were going to have serious problems with sensor drift. Charge mode force sensors are typically used to measure dynamic and “quasi-static” forces. They are not capable of truly static measurements due to a drift caused by charge build up on the transducer that is subsequently discharged through an RC circuit in the charge amplifier. In principle this limits measurements of signals with a time constant of less

than 10 seconds without doing post processing to remove these artifacts. In practice, the signal's time constant needed to be much lower than this in order for us to get a meaningful measurement of small forces in our experiment.

For testing, calibration, and the actual data collection, the voltage output from the charge amplifier was split off to both an oscilloscope and a Kiethley DAS-1200HC 12-bit data acquisition card. We used the oscilloscope to quickly observe signals as we calibrated and adjusted the sensors, while the data acquisition system simultaneously recorded the data for later analysis. Unfortunately, the data acquisition card and LDV hardware would not run under the same operating systems so we could only use one technique at a time.

The calibration procedure we settled upon was to mount the test plate in the empty water tunnel, as it would be during actual runs. From this point we glued a small string to the electrode plate which was then run over a pulley. By attaching a weight to the pulley we could simulate a force similar to drag on the plate. Because of the short time constant and sensor drift, we opted to repeatedly apply and remove the force while the data acquisition hardware recorded the voltage output. To apply the forces, we used a number of large steel nuts that we had weighed previously with a three-beam balance. In this manner, we recorded the force sensor response to 57g, 108g, 160g, and 211g masses.

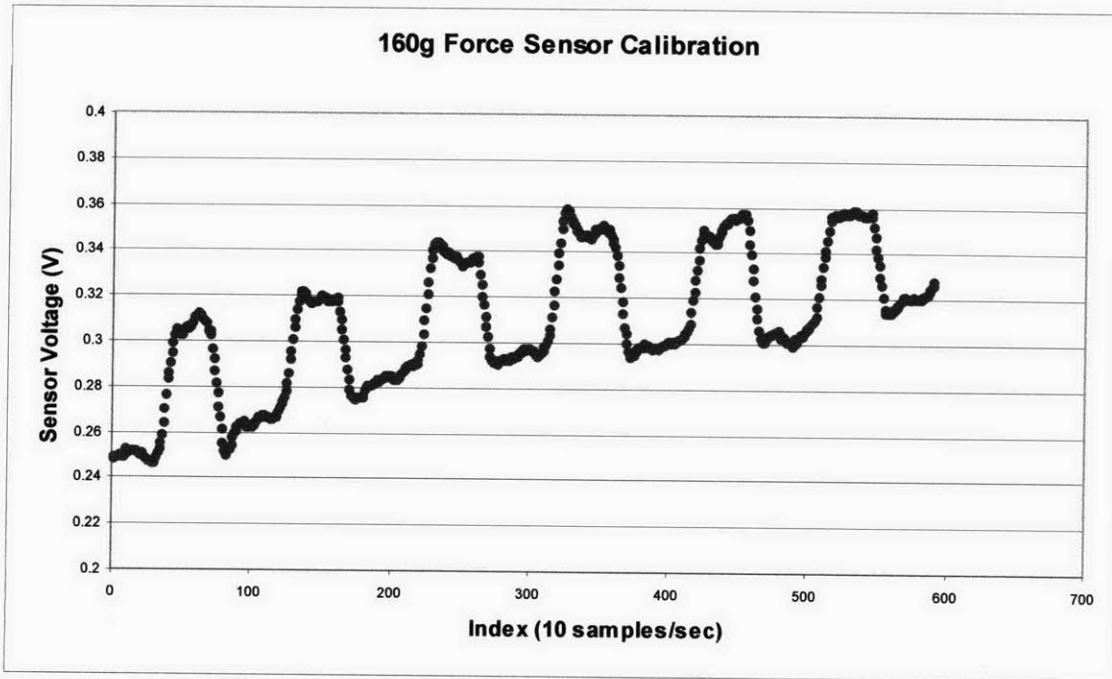


Figure 3-2: Raw data from 160g force sensor calibration in air. The signal results from applying then removing the mass 6 times in succession.

There are several notable features in the calibration plot shown in figure 3-2, the first of which is the rather substantial drift over the 60-second measurement interval. We attempted to eliminate the effects of this drift as well as the inability to measure static loads by accounting for the linear drift and exponential charge decay in software, but failed since the drift was not constant in time. The other point of interest from figure 3-2 is that for many of the calibration signals, the leading edge that corresponds to the force being applied is slightly smaller or less uniform than the recovery when the weight is removed. The reason for this is that in applying the weight, it was necessary to ease it into position to avoid a substantial force that would occur if the weight were allowed to drop into place. Because of this, the average of the voltage changes due to weight removal was the value we used in the calibration calculations as we felt it was more accurate.

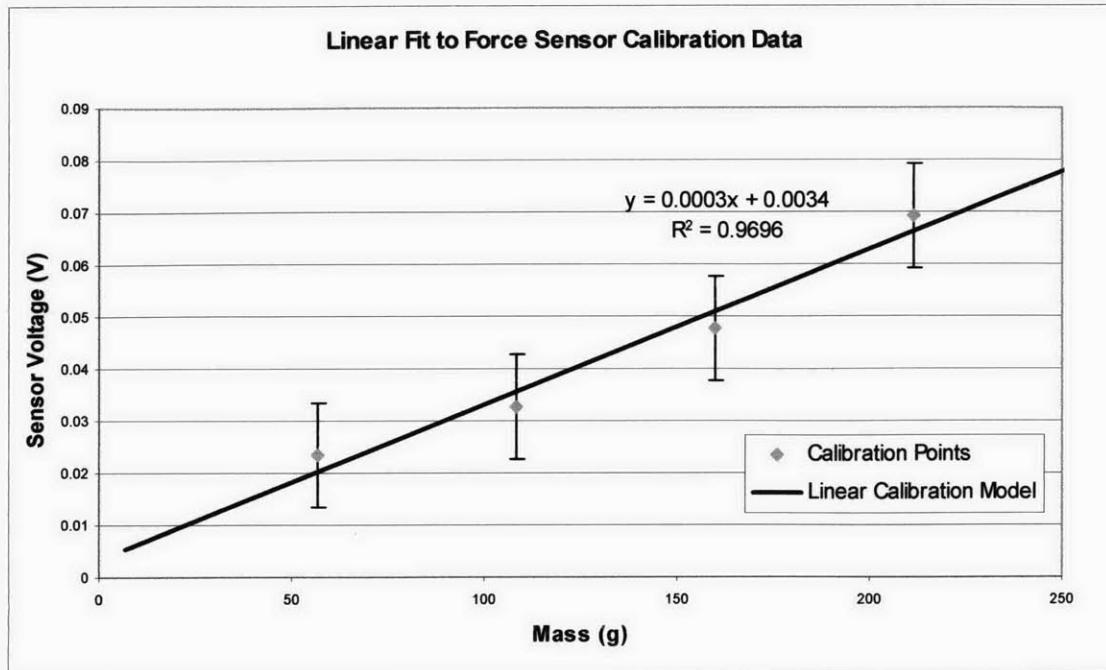


Figure 3-3: Force sensor calibration curve. Estimated error in air was +/- 10mV.

Although calibration in air gave us hope that we would be able to accurately measure forces on the order of those we were interested in, we needed a method to verify that the calibration would remain constant when the sensors were submerged in the sodium nitrite solution. Unfortunately, immediately after filling the tunnel test section, one of the sensors stopped functioning, most likely due to water ingress. Since we still had three sensors in place, we continued with the calibration by sweeping the tunnel velocity from 0 to 3 m/s while recording the force sensor output. Although we had lost our quantitative calibration, we hoped to at least be able to use the force sensors as a qualitative guide to finding the combinations of frequency and amplitude of electrode board excitation that would lead to the greatest drag reduction for the least amount of power.

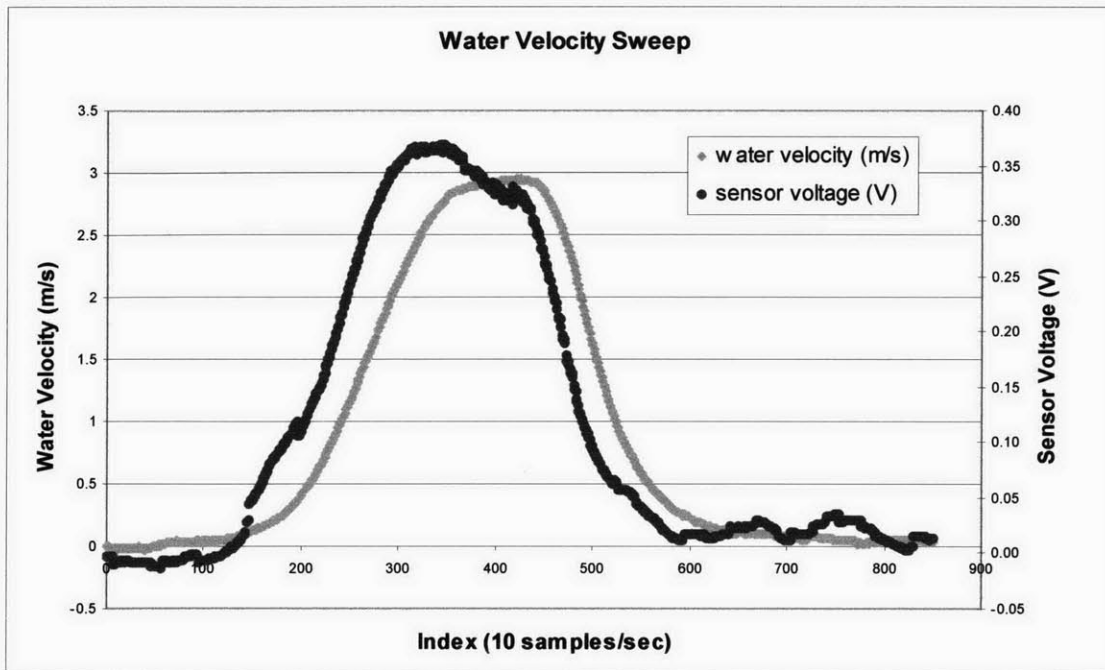


Figure 3-4: Force sensor response to drag on electrode cassette as tunnel speed is varied.

3.3 Results

3.3.1 LDV Measurements

Phase 1 provided us with evidence that we were observing substantial drag reduction for a proper combination of amplitude and frequency. In phase 2, we sought to answer several questions as well as confirm that we were indeed getting drag reduction (as indicated by reduction of du/dy at the wall). The most pressing question to answer was, whether or not we needed to increase the current to get the same degree of drag reduction at higher velocities. The answer to this question is important as it tells us whether or not there will ever be a “break-even” velocity, after which we will get a net energy savings by electromagnetically inducing drag reduction.

In phase 2 we took a total of 38 boundary layer velocity profiles using Laser Doppler Velocimetry. Of these runs, 28 were powered test runs at various frequencies and amplitudes, while the remaining 10 were un-powered baseline cases. As in phase 1, one or more un-powered runs preceded each set of powered runs. For this phase, we concentrated our search around $T^+=100$, which gives the optimal frequency as predicted by direct numerical simulations. Our main thrust was to find the change in the drag, as indicated by the local shear stress, at various amplitudes for water velocities of 1.5 m/s

and 3.0 m/s. At these velocities, the $T^+=100$ frequencies are 56.25Hz and 255Hz respectively. At 1.5 m/s we had significant problems getting well ordered LDV data when running at 10A. The usual linear fit to the first 5 data points in the boundary layer velocity profile had a fit coefficient of $R^2 > 0.95$. However in the 10A run at 56.25 Hz, the best-fit line had $R^2 = 0.79$, by far the lowest of any of the runs. Repeated attempts at measuring the velocity profile for this 10A 56.25Hz case resulted in vastly different data. The 10A data point at 1.5m/s was excluded from the amplitude sweep plot due to this variability.

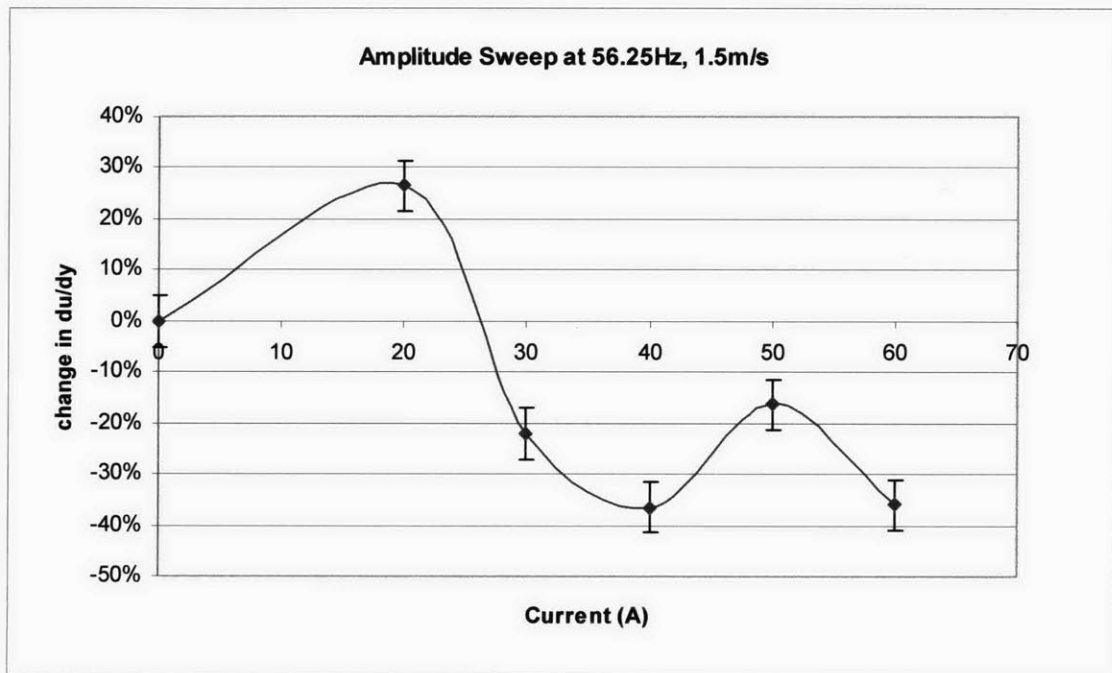


Figure 3-5: Amplitude at 56.25hz, 1.5m/s versus change in du/dy as measured by LDV. The interpolated smooth curve was added to draw attention to the character of the data.

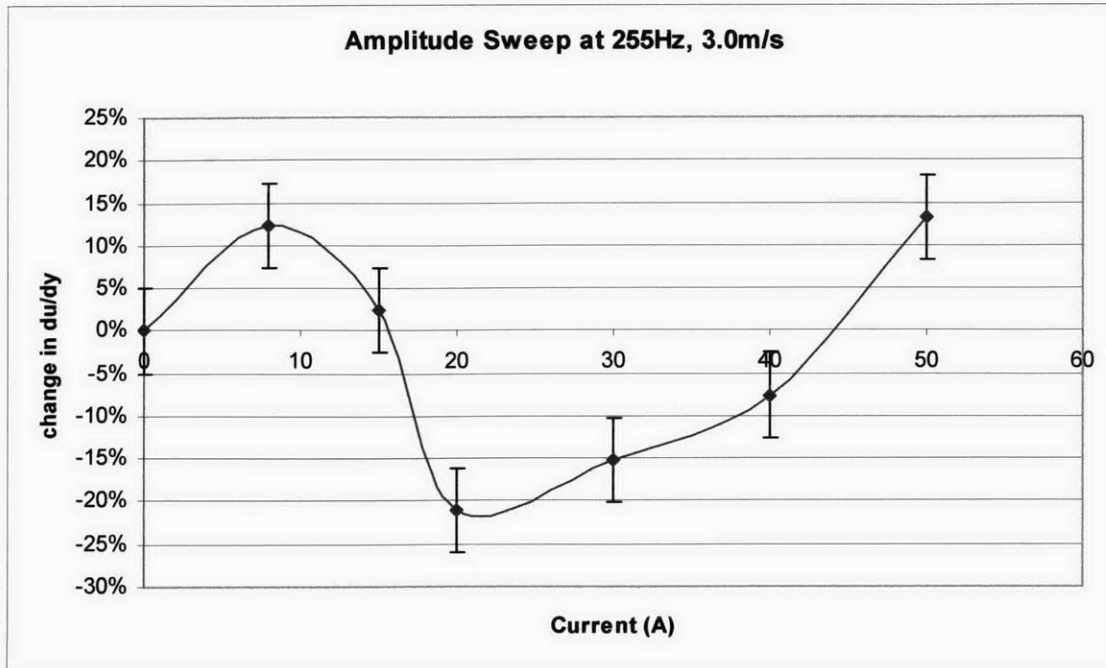


Figure 3-6: Amplitude at 225Hz, 3.0 m/s versus du/dy . The basic structure of the data appears quite similar in many ways to that shown in figure 3-5.

There are many features common to both data sets that are worth pointing out. First, for low amplitudes there is a general increase in the local shear stress at the measurement point. After the initial increase in the shear force, this trend peaks and then declines as amplitude is increased. After the zero crossing (equivalent in du/dy to not powering the electrode array), the local shear stress begins to fall until it reaches a local minimum. The point corresponding to the maximum local shear force reduction is at 40A for the 1.5 m/s case and at 20A when the water velocity is increased to 3.0m/s. Although it is quite difficult to forecast a trend from only two data points, this corresponds to the electrode excitation amplitude varying as the inverse of the velocity, although the local minima are different in both cases (-37% change in du/dy at 1.5 m/s and -21% at 3.0 m/s).

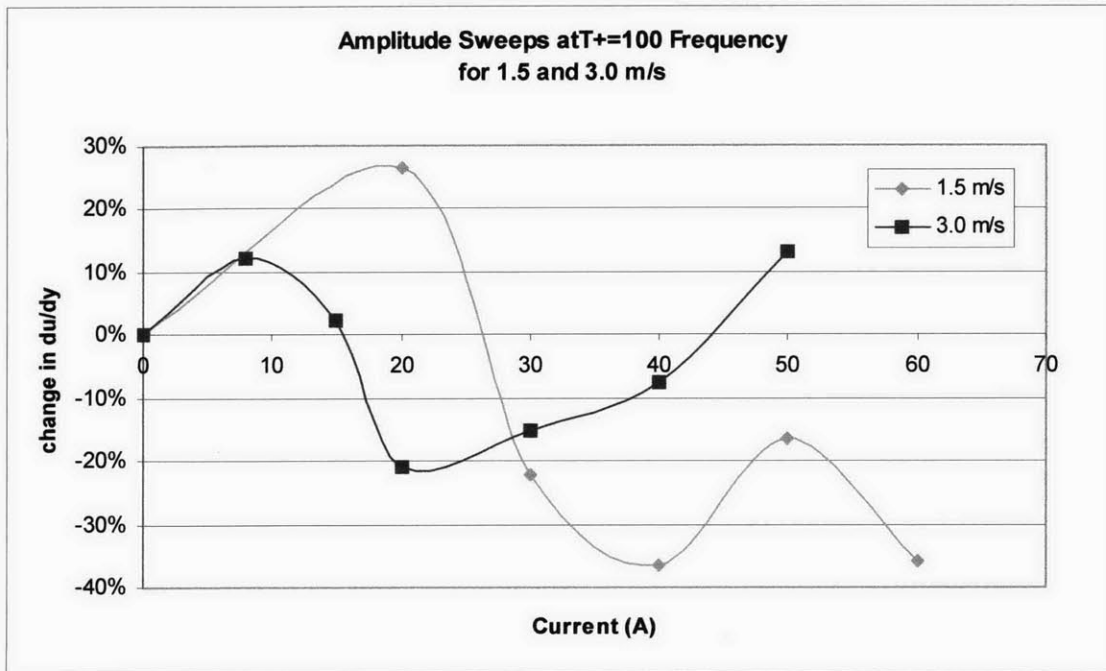


Figure 3-7: Change in local shear stress for $T^+=100$ frequency at both 1.5 m/s and 3.0 m/s.

If this trend continues, the impact on the practicality of this technology would be tremendous. The main problem with inducing drag reduction using Lorentz force actuation is that there is quite a bit of energy used to excite the electrode array and fairly little energy saved by reducing drag at low velocities. For example, by reducing the drag on our plate by 30% at 3 m/s, we would reduce the force on the plate by about 0.62 N (64g). This drag reduction corresponds to an energy savings of 1.9 W, while we expend $20A \cdot 6.3V = 126W$ in energizing the electrodes. This ratio of power input to power saved through drag reduction corresponds to an efficiency of about 0.015 at 3 m/s. Although this looks fairly grim, the power loss due to drag increases as the cube of the water velocity. With this fact, even if the power requirements of 420W stayed the same as the 1.5 m/s case, but we assume we can still achieve approximately 30% reduction at any velocity for the appropriate frequency, we would expect to reach a break-even point at 18.3 m/s after which we would experience a net energy savings. However, if the inverse relationship between velocity and excitation amplitude continues, we would reach the break even point at about 8.2 m/s where we would be getting a 38 W power savings due

to drag reduction and using 38 W for electrode array excitation if we continue to see approximately 30% reduction in drag at any velocity. Forecasting this trend forwards suggests that at 10 m/s we would see an efficiency of 220%.

In addition to the amplitude sweeps at 1.5 m/s and 3.0 m/s, we did a similar sweep at 1.28 m/s. However, the operating frequency was 30Hz, corresponding approximately to $T^+=135$ instead of $T^+=100$. It will take considerably more investigation to see how this shift in frequency affects the optimal current and efficiency, but the results have many similarities in character to the previous amplitude sweeps with the exception of a smaller reduction in the local shear stress.

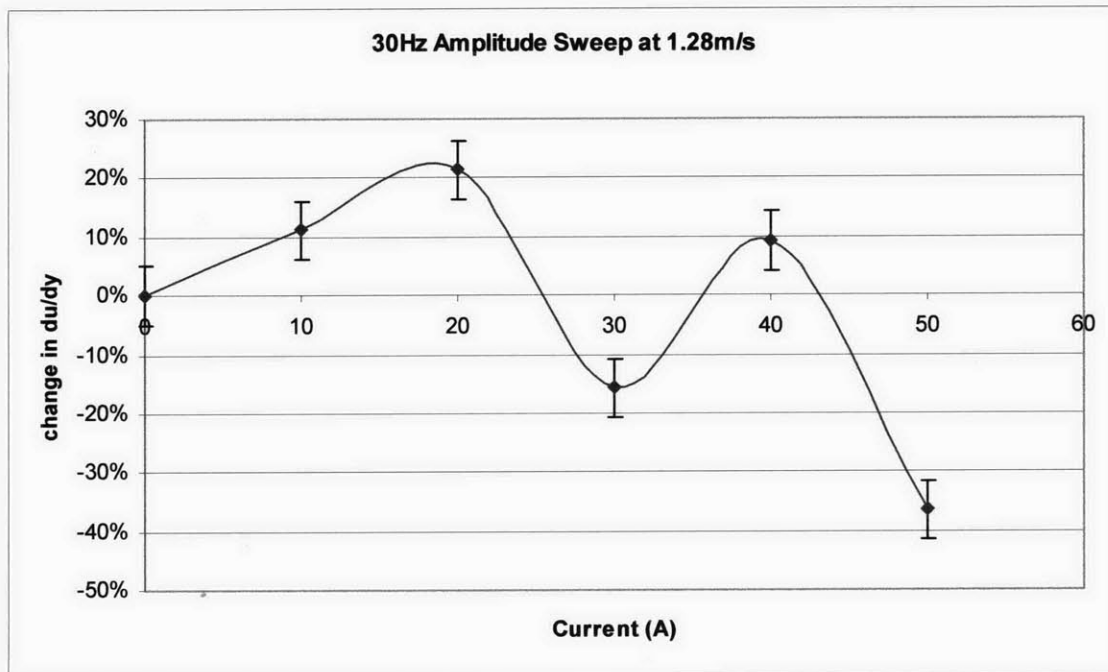


Figure 3-8: Amplitude sweep at 30Hz ($T^+=135$), 1.28 m/s.

A final notable result is that we were able to observe significant changes in the local shear stress at any velocity even though our electrodes were quite a bit larger than the optimal electrodes predicted by the numerical simulations. The parameter that is altered by the electrode width is the penetration depth of the force into the boundary layer. In the numerical simulations, this is characterized as the electrode width divided by π in the simplest case. The optimal electrode width according to the direct numerical simulations is between 10 and 20 wall units, which corresponds to a penetration depth of about 0.13mm at 1 m/s. The electrodes in our array were 3.175mm (.125") wide, which

gives a penetration depth of 1.01mm. The fact that we still get the change in du/dy predicted by the numerical simulations is fortuitous since dealing with electrodes and magnets as small as predicted necessary by the simulations would be problematic.

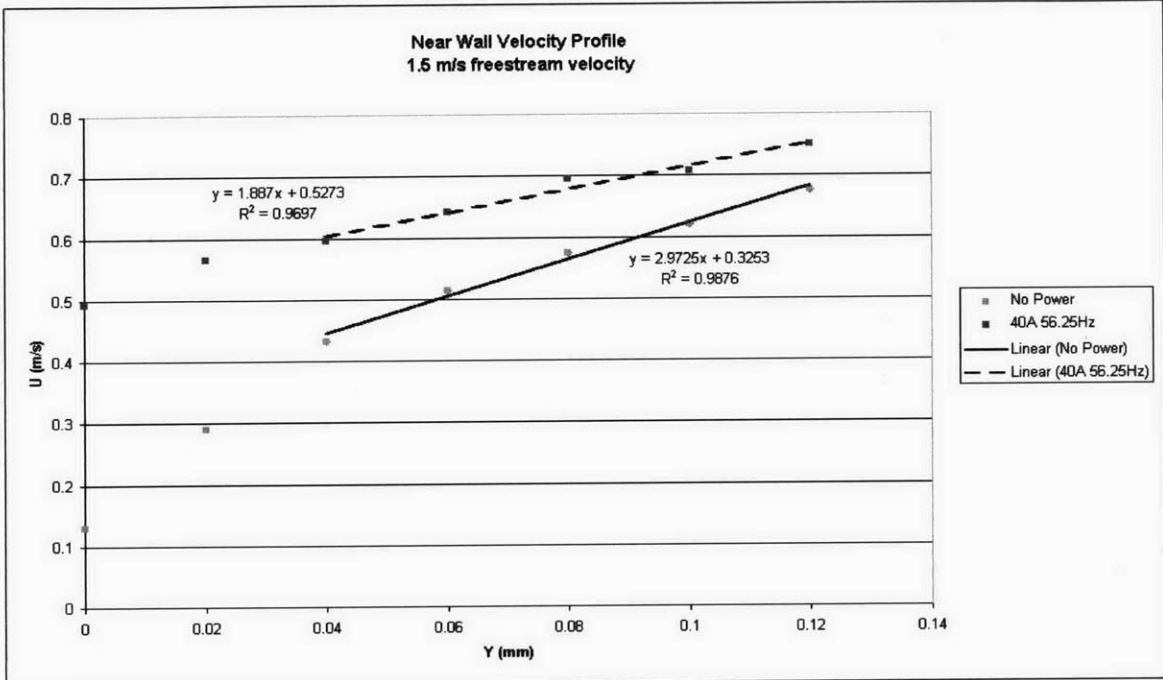


Figure 3-9: Near wall velocity profile at $T+=100$ frequency for 1.5 m/s. The trend lines are fit to the 5 points nearest them. Error estimates are omitted for visual clarity but are +/- 5% of the freestream velocity.

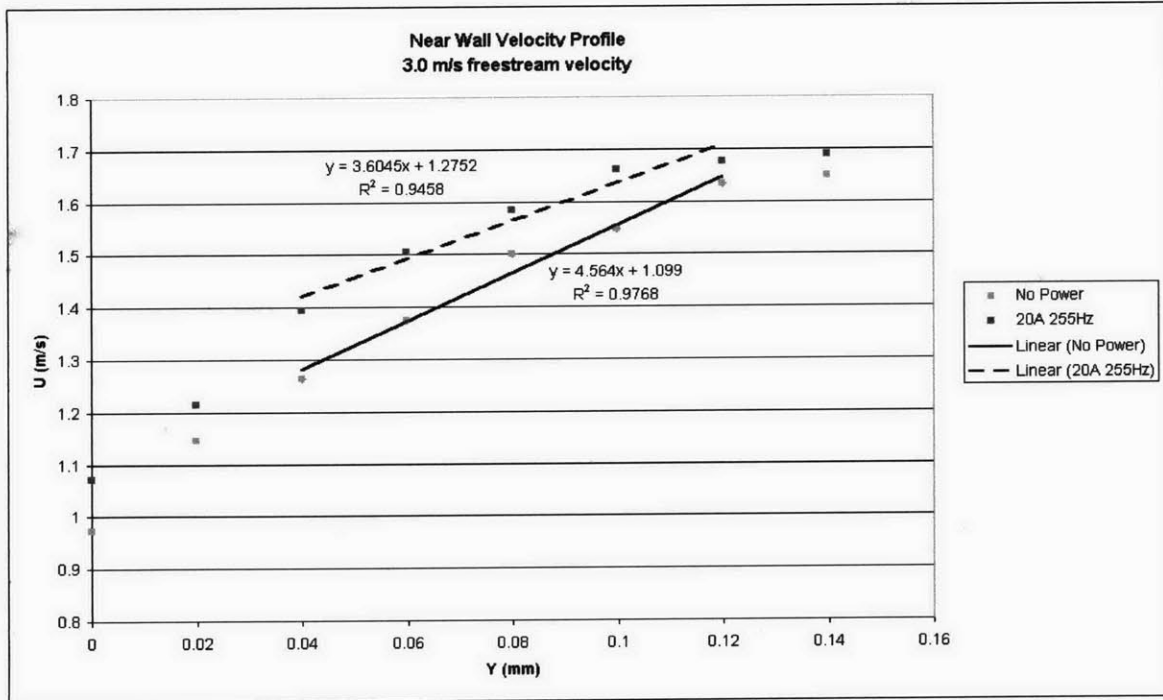


Figure 3-10: Near wall velocity profile at $T+=100$ frequency for 3.0 m/s.

3.3.2 Direct Force Measurements

We had a great deal of difficulty getting the direct force measurements using the piezoelectric shear force sensors. However, due to the appealing prospect of measuring forces much more quickly than by using LDV as well as the capability of measuring the total drag on the electrode plate, we spent a considerable amount of time attempting to get this solution to work.

After losing one of the four sensors immediately upon filling of the tunnel, we had decided to quickly take a few representative sweeps in frequency and amplitude while the remaining three sensors were still functional. As noted in the experiment design section, losing a sensor destroyed our original calibration curve, but we hoped to still get a qualitative mapping of drag change at various frequencies and amplitudes. Of course, if the sensors did not experience any degradation during their submergence, we could again repeat the calibration procedure to account for the failed sensor in a new calibration curve. Unfortunately, the sensor parameters changed enough while we were doing the qualitative mappings that it was impossible to relate these values back to an actual value for drag on the plate.

The biggest issue in working with these sensors was, by far, the drift characteristics. Our testing in air confirmed that we would only be capable of measuring signals with a time constant less than about 10 seconds due to the decay circuitry in the charge amplifier and that if care was not taken, the zero force signal would drift out of range ($\pm 5V$) over the course of several minutes. However, once submerged in the sodium nitrite solution, the drift rate became significantly worse. In practice we only had about 10 seconds from the time the charge amplifier was activated to make a measurement before the drift would take the voltage signal out of range. The direction of the drift when the sensors were submerged seemed to be heavily in the negative direction, while in air the drift direction was approximately random over time. The constant direction and large amount of drift led us to hypothesize that the ingress of the conductive sodium nitrite solution into the sensor housings was causing a change in the charge build up and removal rate when compared to operation in air.

To cope with the short time we would have to make a measurement due to the drift rate, we decided on a procedure that would allow us to calculate the drift rate for

each sample as well as take actual force sensor data for a single frequency-amplitude pair within a few seconds. To do this, we would bring the water velocity up to the desired velocity (we used 3 m/s in order to increase the drag force) and then take baseline data for a few seconds after the velocity stabilized. Without interrupting data collection, the power electronics, which were previously set to the frequency and amplitude of interest, were turned on for several seconds to activate the electrode array. After turning off the power electronics, baseline data was again taken. If the signal was not in danger of drifting below the $-5V$ that we could measure with the DAS-1200HC data acquisition board, we would repeat the cycling of power to the electrode array. By using the baseline data from before and after the actual measurements, we were able to calculate the drift and account for it by shifting our collected data by the appropriate linear function. In this fashion, we swept through the amplitude parameter space by changing the current supplied to the electrode plate between each set of direct force measurements.

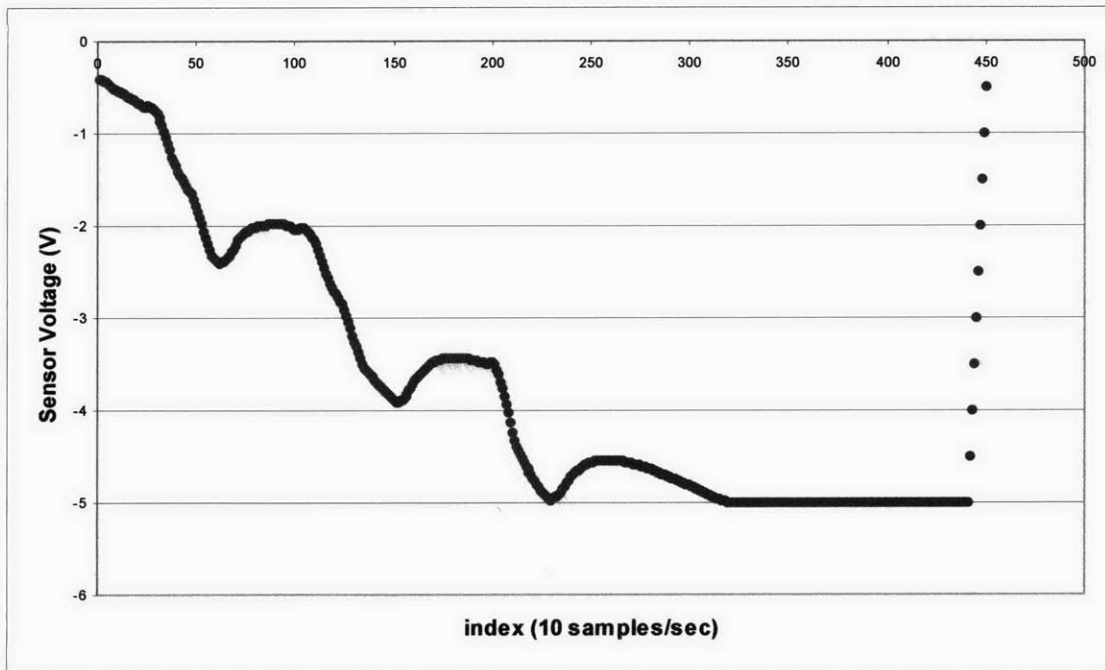


Figure 3-11: Raw force sensor voltage data after the charge amplifier signal was passed through the filter and gain modules. The amount of drift is obvious, along with the signal going out of range at $-5V$. The points extending back to zero volts are artifacts of the 10 point rolling average that was used to help clean up the data.

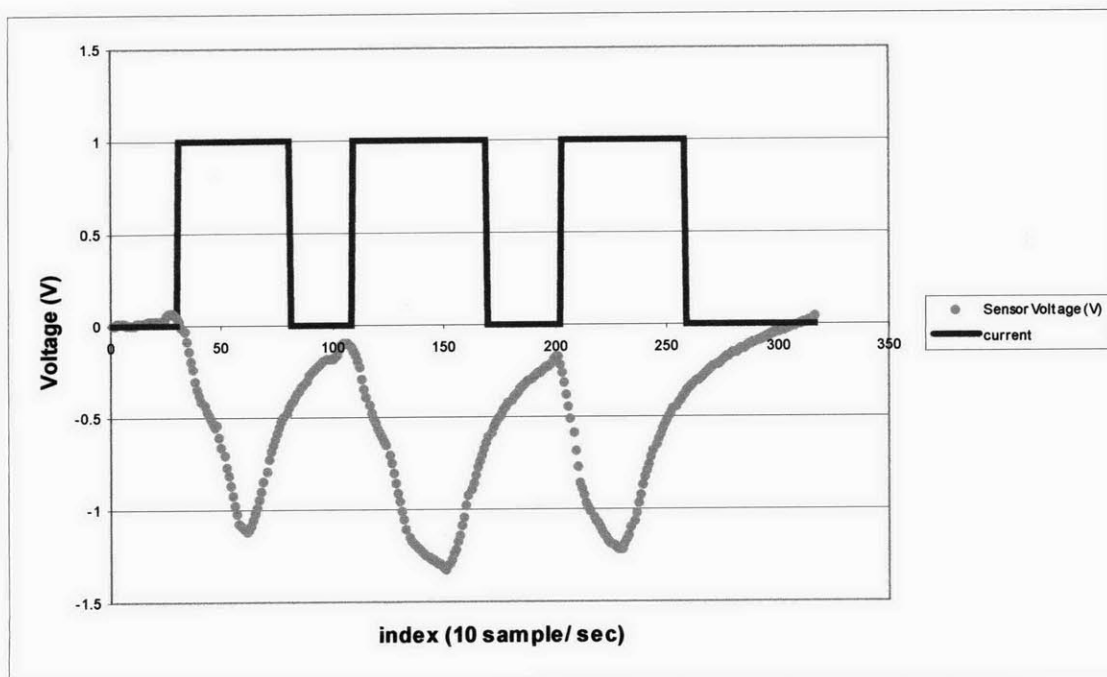


Figure 3-12: Sensor voltage after linear drift was removed. The normalized current data shows when the electrode array was activated.

Because of the very short time we had to make a measurement before the drift would take the signal out of our range of measurement, we never had to deal with the exponential decay of the force signal due to the charge amplifier's discharge circuitry. However, we did have several other sources of noise that we removed in order to get cleaner data. Initially, the biggest source of noise was 60Hz oscillations due to the pickup of the wall potentials by the force sensor cabling which was strung through the air for about five feet between the test section and summing box. To remove this signal, we passed the voltage output from the charge amplifier through a Krohn-Hite Model 3384 filter module configured as an 8-pole low-pass Butterworth filter with a 20Hz cutoff frequency. In addition the filter unit had an adjustable output gain module that allowed us to amplify the output signal. To attempt to minimize the drift issues we reduced the gain of the charge amplifier and added the gain back in with the filter bank module to alleviate the possibility that the problem had more to do with the charge amplifier electronics than the actual charge build up on the force sensors. Although this seemed to help a little, the effect was not remarkable.

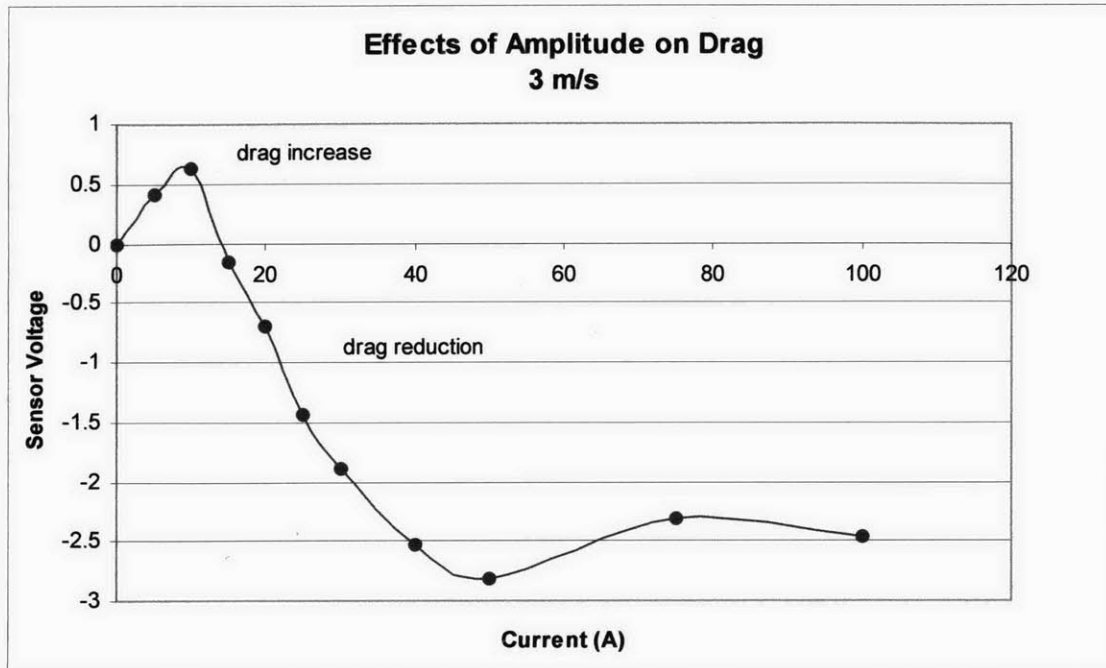


Figure 3-13: Average force sensor data from each current level that was tested. Although this sweep was done at 30Hz ($T+=750$) to investigate the effect of frequency, many of the features are similar to the LDV amplitude sweep at $T+=100$ for 3 m/s. Error bars are not present as it was impossible to estimate the amount of error do to the various factors, but it was likely quite high.

After taking the original amplitude sweep with the force sensors, we waited several days before performing additional force gauge measurements as we focused on getting boundary layer velocity profiles with the LDV system. Upon retesting the force sensors, we found that there were very high noise levels present on top of the drift. After a night of investigation, we finally realized that the sensors were displaying high amplitude oscillations at the operating frequency of the electrode array. Unfortunately, with the 20Hz cutoff low-pass filter bank in place, this effect was initially obscured. In addition, our original data was taken at a 10Hz sample rate by the data acquisition board, which would have aliased any signals above about 5Hz. Because of this oversight, it is difficult to be certain that this interference was not always present from the moment the sensors were submerged, but this effect was not observed on the oscilloscope, which was displaying the force signals during most of the early experiments without the filter module. My personal inclination is that after the conductive solution leaked into either the sensors or their cabling after days of immersion, this effect became present.

Even though it was clear that the signal was being completely overwhelmed by the noise at the fundamental operating frequency, we attempted to do another drag versus amplitude sweep. For this run, the 8-pole filter was removed and the sample rate was increased to several times over the operating frequency. The sampling rate was also set to a prime number in each case to alleviate the possibility of perfect aliasing. The way we took the data was the same as in the original force sensor amplitude sweep discussed above, but this time after the original amplitude change the signal would oscillate at the operating frequency.

Although we felt that any effects due to drag changes would be obscured by the electrical noise, it was surprising how closely this amplitude sweep matched the original. This could, of course, mean that the same noise effects were present in the original sweep and that in both cases the data has nothing to do with drag on the plate. However, the clear similarities between the force measurements and LDV sweeps from figures 3-7, 3-8, and 3-9 suggest that we were indeed measuring the effects of drag. In any case, we were not able to measure the amount of force on the plate as a quantitative value, but it looks likely that these sensors will allow for qualitative investigations of large parameter spaces at a much faster rate than could be accomplished by LDV measurements.

4. Conclusions and Future Work

4.1 Conclusions

We successfully implemented a Lorentz force actuator array and used it to validate the drag reduction predicted by extensive numerical simulations. In the first phase of our investigation, we confirmed that this technique is capable of reducing the local shear stress at a measurement point. In the second phase we instrumented the test plate with piezoelectric direct force sensors in an attempt to confirm that the change in the local shear forces (du/dy) measured with Laser Doppler Velocimetry corresponded to actual drag reduction across the entire electrode array. Although the force sensor measurements supported this conclusion, there were significant problems with noise and drift in the force sensors that prevent us from stating that we observed overall drag reduction with absolute certainty. Also in the second phase, we repeated the LDV measurements of the first phase at several different velocities and confirmed that for the proper combinations of amplitude and frequency, we can achieve over 30% reduction in the local shear stress. Efficiency calculations based on the results of both phases indicate that although we used over 60 times the power we could save at 3 m/s, the dependence of power loss due to drag on the cube of velocity may give us a break-even efficiency at as little as 8.2 m/s.

4.2 Contributions of This Work

The main contribution of this work was the experimental implementation of the drag reduction technique based on spanwise excitation using Lorentz force actuators. This work is substantially different than many other drag control techniques in that it focuses on creating spanwise vorticity instead of streamwise manipulations common to most of the other control techniques. This work also differs from the spanwise control methods implemented by researchers, such as those at Brown University, in that it uses an oscillating square wave instead of a traveling sinusoid for the electrode array excitation. In addition, this investigation was carried out in a water tunnel instead of in a channel-flow and incorporated both Laser Doppler Velocimetry measurements as well as direct force measurements with piezoelectric sensors.

4.3 Future Work

There are several potential ways in which this research could be constructively continued. The most obvious is to continue testing, characterizing, and optimizing the effect. In my eyes, this is worth a substantial investment in time and funding before moving to the practical embodiments of this technology such as implementing it on an AUV or other real world test platform. Since we will likely need to operate at velocities higher than that at which we have been testing in order to gain an efficiency of greater than unity; high velocity testing seems the next logical step for this work.

Initially, the high velocity testing could use the same electrode boards and test plate, but care would have to be taken to make sure the apparatus can physically sustain the forces present during high-speed runs. A positive side of running at high velocities is that the direct force measurements will be significantly easier to perform as the drag forces will be on the order of pounds instead of grams as it is in the 1.5 m/s regime. As we were working at the absolute lowest sensing range of the piezoelectric force transducers during our 1.5 m/s tests, the granularity of the force measurements would be significantly reduced. Also, increasing the drag force significantly may make it more feasible to attempt to use more traditional direct force sensing techniques and abandon the fickle piezoelectric sensors altogether.

If the high velocity path is taken, the initial equipment costs can be kept minimal. At the minimum we will need to purchase a power supply (ours is on loan), coated electrode boards, a few (50) more magnets to replace any corroded ones, and printed circuit boards for the switching circuitry. The switching circuit is currently laid out on two temporary breadboards. This solution is adequate for our current testing, but is not viable in the long run, as it is not very permanent or well documented. Embodying this knowledge in a PCB design would alleviate this problem.

If the high speed testing path is pursued, there will need to be many more boundary layer velocity profiles measured using LDV to be certain of how the change in the local shear stress varies with amplitude and water velocity. This is perhaps the most important part of the investigation to continue since it will indicate the efficiency of this technique at higher speeds. Aside from single LDV cuts, the slope of the velocity profile near the wall should be taken at several points along the streamwise direction of the

electrode plate to validate that we are seeing overall drag reduction and not a decrease in du/dy at one point followed by a corresponding large (or larger) increase in the local shear on the rest of the electrode plate.

Additional direct force measurements could be substituted for these LDV measurements if the reliability and sensitivity of the force measurement solution was improved. One option for improving the force measurements is of course to attempt to implement a more traditional pendulum or strain gauge technique. However, I still believe there is hope for the piezoelectric sensors. In my opinion, waterproofing both the sensors and their attached cabling with much care will alleviate many of the problems we experienced with the submerged sensors. In addition to this environmental protection, removal of the linear drift, exponential decay, and sinusoidal noise induced by the electrode activation can be accomplished in software. We made attempts to implement a software solution as described using Labview to analyze and process the data, but did not have much success due to the highly increased drift and noise problems we had after submerging the sensors. Our experiences have shown that any attempts at removing these artifacts will need to be dynamic in that it would need to calculate the slope of the drift rate and period of the electrical noise signal for each measurement. However, cursory testing has suggested that the exponential decay caused by the RC circuitry in the charge amplifier has a time constant close to that indicated by the amplifier documentation so this could probably be a static compensation function, depending only on the settings of the charge amplifier.

Another viable research thrust would be to attempt to optimize the induced drag reduction by varying the current waveform and distribution across the electrode boards. This can be done in several ways including the traveling wave design originally proposed by George Karniadakis. Kenny Breuer's group at Brown University has had success with this technique at low speeds. Between the two possible ways of making changes to the electric field, changing the electrode distribution is much less expensive and research intensive than changing the switching technology. Unfortunately, to induce traveling waves it will probably be necessary to change both the electrode board design as well as the power electronics. In my opinion, this line of research should be pursued at a later time if working towards an application based technology is the goal since the square

current waves seem to be producing about 30% drag reduction and are by far the simplest implementation.

On the other hand, there are several simple modifications that could be made to our waveform in order to attempt to enhance the effect and to reduce the power expenditure. The easiest change to our setup that would allow us to explore other waveforms would be the addition of a fifth (the h-bridge uses 4) IGBT or FET switch in the positive power cable that leads to the electrode array. By doing this we could have an off state in our waveform instead of only positive or negative potentials as our electronics demand currently. This addition would allow us to explore a large range of different pulse width modulated and pulse train signals that could still swing both positive and negative. Even if no waveform other than the constant amplitude plus/minus waveform that we are currently using produced an effect, we could still use the additional switch to turn the power to the electrode array off for short times. The reasoning behind this concept is that there is certainly some finite response time faster than which the drag on the plate cannot return to normal once it has been reduced by the spanwise actuation. If we deactivate the electrode array for a shorter time than this response time we could experience considerable power savings. The idea of switching the unit on and off at set intervals while taking drag data is also equivalent to investigating the distance by which electrode panels could be separated on a large surface before the turbulence is reestablished between the plates. Answering this question will allow us to determine if an underwater body would need to be “wallpapered” with these electrode tiles or if strategic location of tiles spaced along the surface could accomplish the same effect while using much less power.

Another research path to consider is attempting to integrate the actuators in a real world application. I personally feel that the high velocity water tunnel testing should take precedence over this, but if funding allows, it would be encouraging to start this work in parallel. The initial costs of building this technology into an AUV or other test platform could be quite high due to several design and implementation issues. However, careful consideration may mitigate some of these problems.

These costs would mostly be due to attempting to translate the flat plate mechanism into an analogous concept for an axis symmetric body. To illustrate this

problem, consider a physical analog to the forces being produced by the interplay of the electric and magnetic fields on the flat plate. Since the forces are perpendicular to the flow direction and abruptly change direction every half cycle, the effect is exactly the same as holding the edge of the plate and sliding it quickly back and forth perpendicular to the flow. The distance which you translate the plate is related to the current density of the electrode array and the speed at which you translate it is analogous to the switching frequency. To extend these concepts to a cylindrical body, we would have to alter how we were moving the body through the water to induce the drag reduction. In the case of the cylindrical body we would need to use the Lorentz forces to perform the equivalent of rotating the body about its axis. This would be somewhat similar to the numerically modeled [9] case of rotating a pipe through which a fluid flows, but in our case, the fluid is on the outside. Although the amplitude and frequency analogies would be the same as in the flat plate example, we would now need a significantly more complex arrangement of the magnetic and electric fields. For the most part this would need to be accomplished by careful consideration of how the magnets would be placed on the body and how the electric fields were shaped through both electrode placement and switching techniques. With respect to the magnets, there are several known techniques of embedding magnets in a plate that may help here (for example the EMHD plate used at Brown University has .4 Tesla Neodymium Iron Boron magnets embedded in the electrode tile) but it will probably not be as simple as just arranging magnets around the surface of the body since there will then be a substantial interaction between adjacent magnets in a way that was not present in the flat plate tests.

If the application based route is still pursued regardless of these challenges, there are several methods that could be used to reduce the complexity and variance from the flat plate design. The first method, although most likely prohibitively expensive, would be to install a large array of these tiles on a cylindrical body with as large a radius as possible (e.g. a nuclear submarine). With a large radius each square foot section that would be occupied by the standard electrode boards would be approximately flat, thus enabling the same magnet configuration and current control techniques. A more practical solution may be to make very small actuator tiles (perhaps only one square inch or so). If

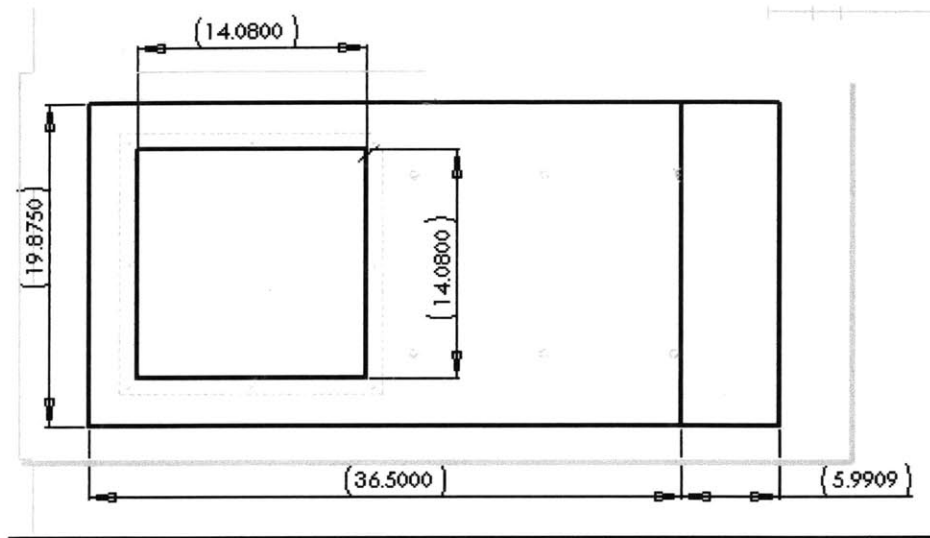
many of these tiny tiles were affixed to a cylindrical body the size of an AUV or torpedo, they would each occupy a region that was locally nearly flat.

A final possibility for the applied testing would be to design a test vehicle with a cylindrical nose but planar sides. The flat sides could then have the standard electrode plates installed. Although this would allow us to use the electrode plates and control circuitry that we have gained considerable confidence in, much of the drag on the body would be at the nose where we would not have any tiles in place. The costs associated with real world testing are hard to ascertain but would likely include all of the equipment costs from the high speed testing in addition to a considerable expenditure on design and implementation. This route would probably require at least two graduate students from mechanical or ocean engineering as well as one or two graduate students or postdocs from electrical engineering.

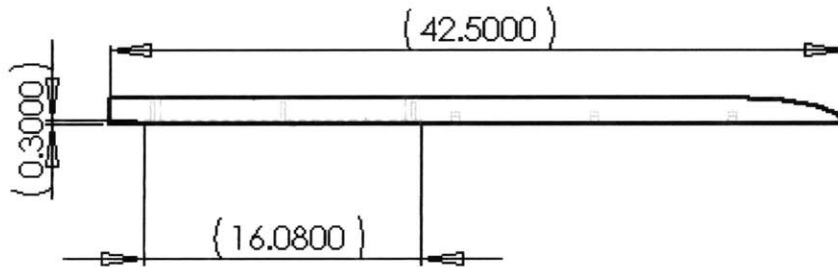
References

- [1] Karniadakis, G. & Choi, K. Mechanisms on transverse motions in turbulent wall flows. 2002 Annu. Rev. Fluid Mech.
- [2] Du, Y., Symeonidis, V. & Karniadakis, G. E. . Drag reduction in wall-bounded turbulence via a transverse traveling wave. Journal of Fluid Mechanics 457,1-34.
- [3] Y. Du and G.E. Karniadakis, Suppressing wall turbulence by means of a transverse traveling wave, 2000 Science 288, 1230.
- [4] Berger, T. W., Kim, J., Lee,C. & Lim, J. 2000 Turbulent boundary layer control utilizing the Lorentz force. Phys. Fluids 12(3), 631-649.
- [5] Du, Y., Beskok, A. & Karniadakis, G. E. Simulations of a Lorentz force actuator, Center for Fluid Mechanics #98-25.
- [6] Kassakian, John G. , Schlecht, Martin F., & Verghese, George C.. Principles of Power Electronics. Addison-Wesley, 1992.
- [7] Power Transistor Module & Accessory Product Guide. Powerex, 2000.
- [8] Schlichting, H. & Gersten, K. Boundary Layer Theory. Springer,2000.
- [9] Quadrio, M. & Sibilla, S. 2000 Numerical simulation of turbulent flow in a pipe oscillating around its axis. J. Fluid Mech. 424, 217-241.
- [10] George Karniadakis. Personal communication, May 2002.

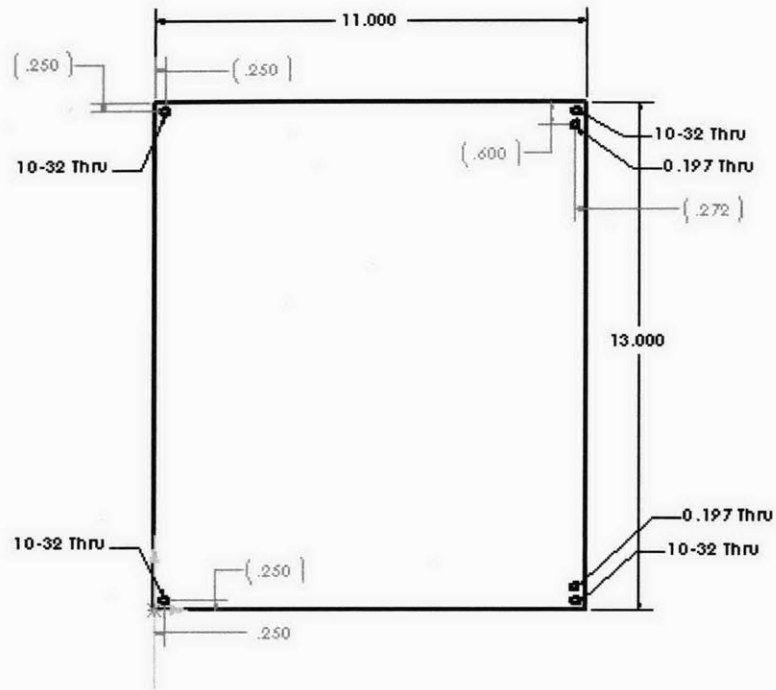
Appendix



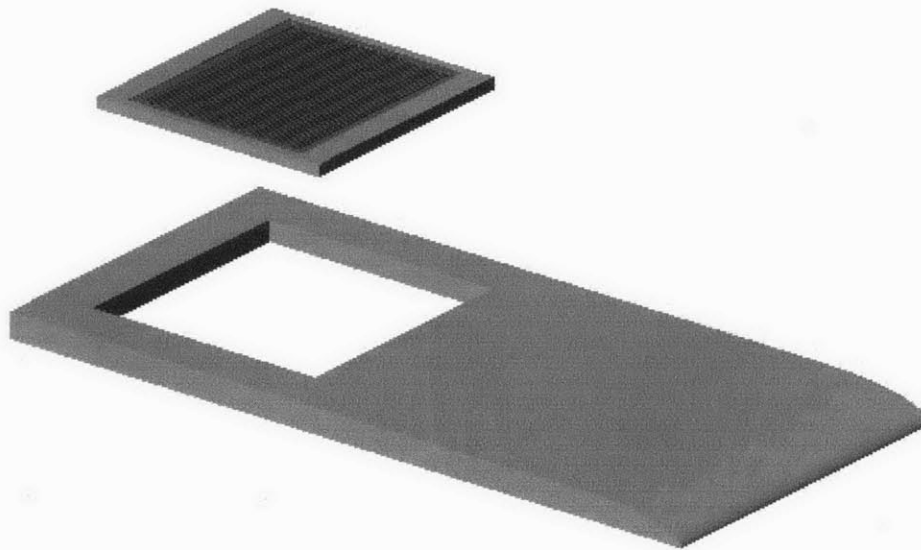
Delrin test plate with electrode area cut out for phase 2.



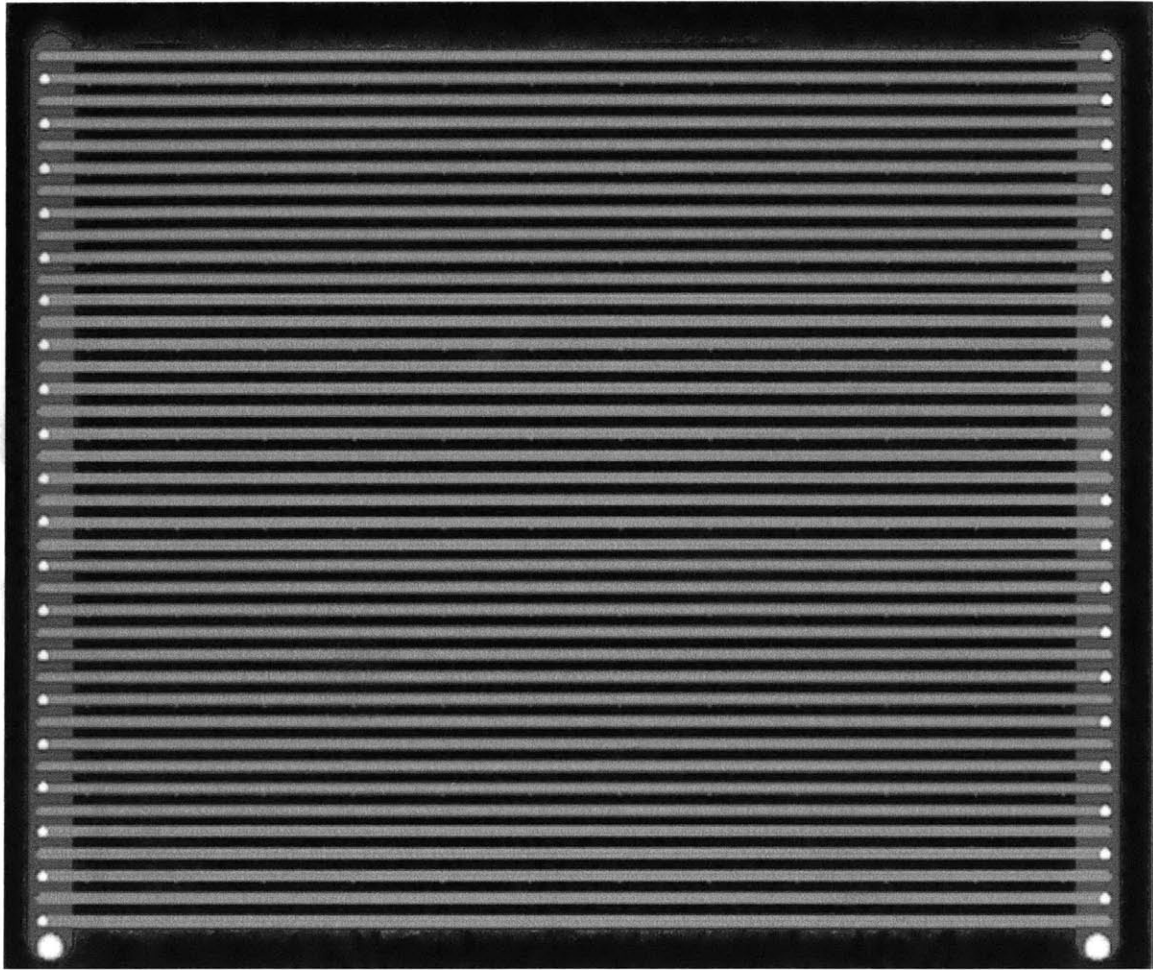
Side view of test plate.



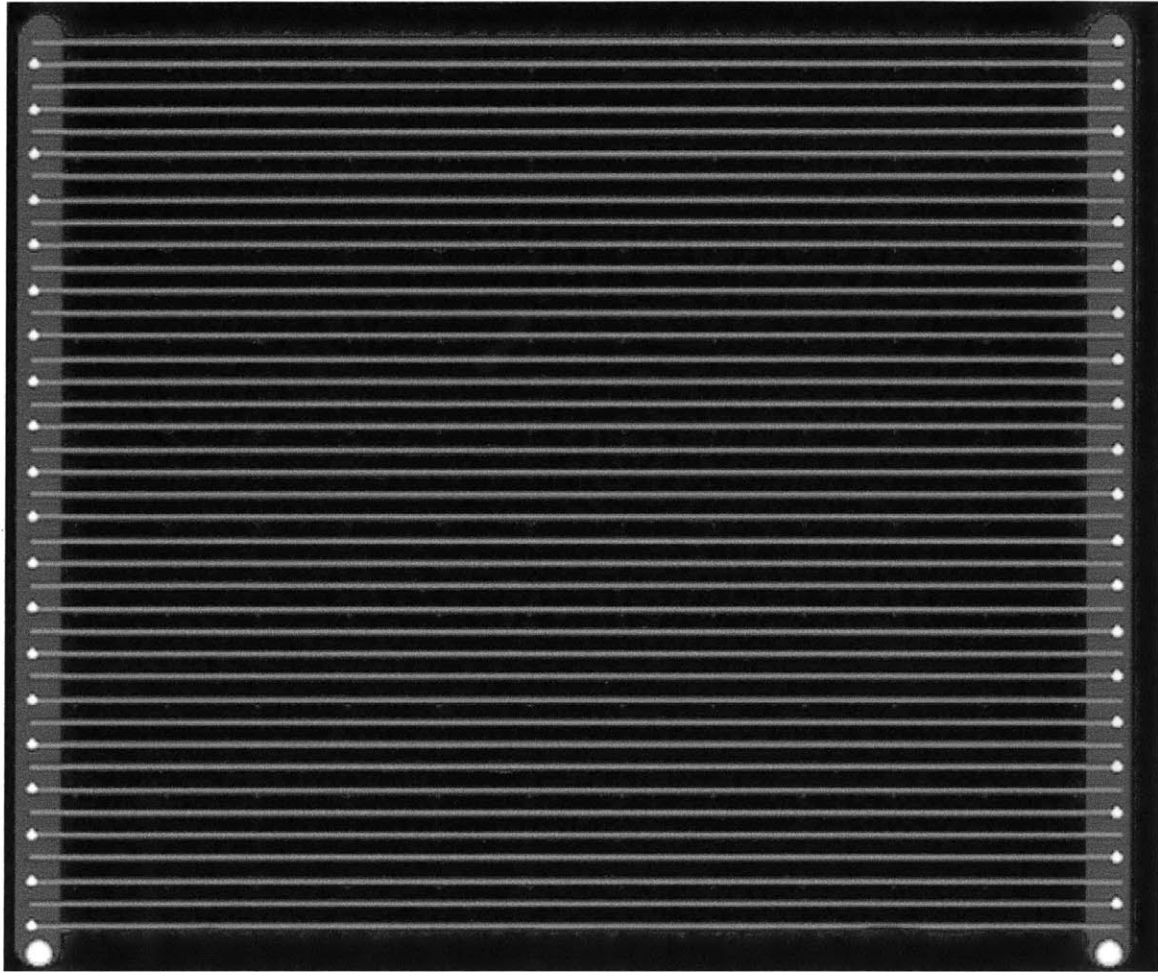
Magnet backplate.



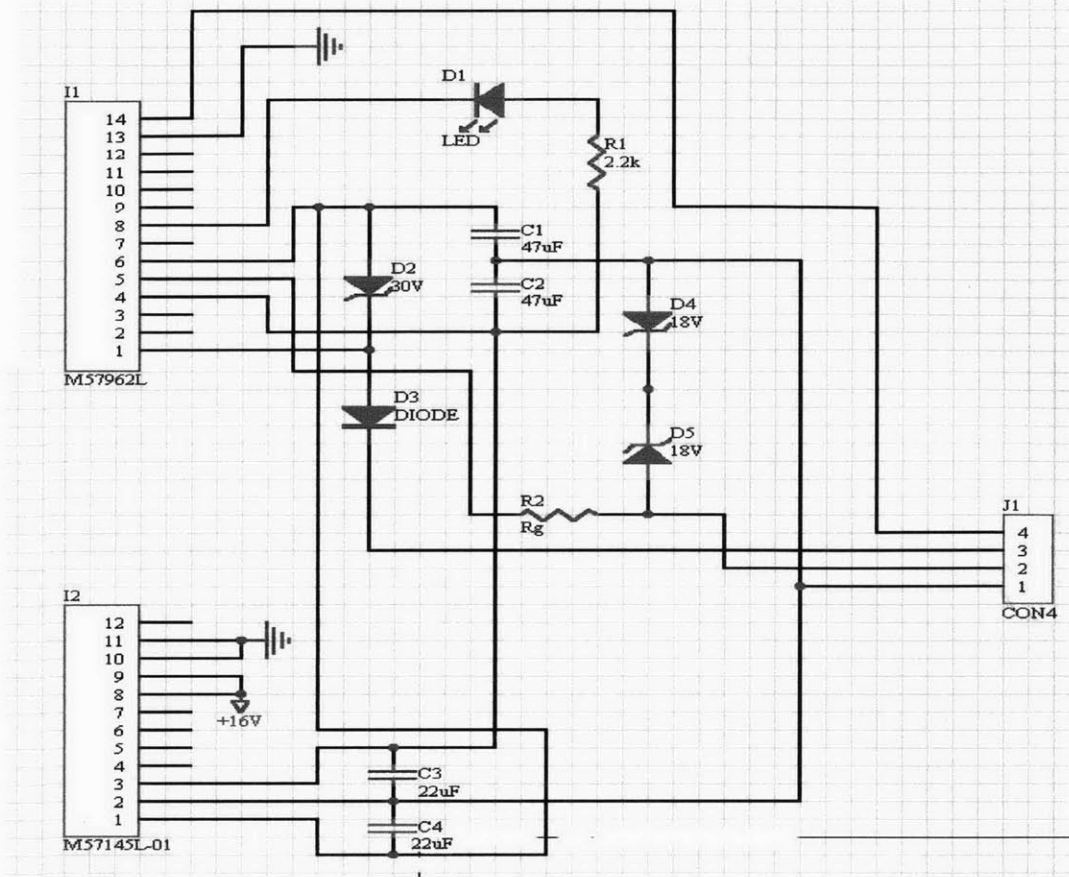
Test plate with removable electrode cassette.



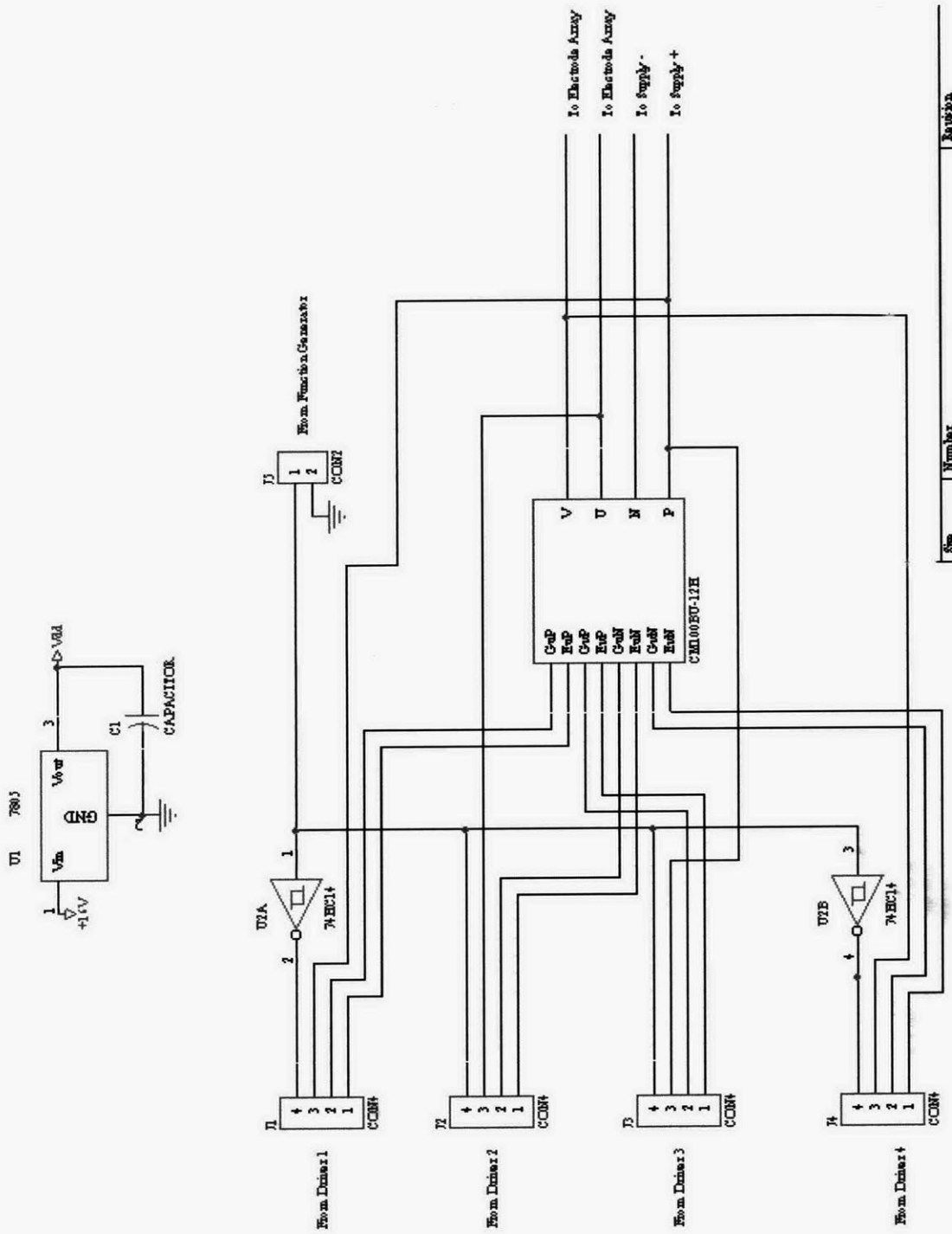
Large electrode plate, 1:2 reproduction. The thick tracks are on the bottom layer while the thinner traces that form the 40 electrodes are on the top layer. The white circles are plated through holes.



Electrode board with thinner electrodes, 1:2 reproduction.



IGBT driver schematic.



IGBT switcher schematic.